

Dear Author

Please use this PDF proof to check the layout of your article. If you would like any changes to be made to the layout, you can leave instructions in the online proofing interface. Making your changes directly in the online proofing interface is the quickest, easiest way to correct and submit your proof. Please note that changes made to the article in the online proofing interface will be added to the article before publication, but are not reflected in this PDF proof.

If you would prefer to submit your corrections by annotating the PDF proof, please download and submit an annotatable PDF proof by clicking [here](#) and you'll be redirected to our PDF Proofing system.

Available online at www.sciencedirect.com

jmr&t
Journal of Materials Research and Technology

<https://www.journals.elsevier.com/journal-of-materials-research-and-technology>


Review Article

Review: Achieving enhanced plasticity of magnesium alloys blew recrystallization temperature through various texture control methods

Lifei Wang^{a,*}, Yongqiao Li^a, Hua Zhang^b, Zhengyong Zhang^a, Qingshan Yang^c,
Qiang Zhang^a, Hongxia Wang^a, Weili Cheng^a, Kwang Seon Shin^d, Maurizio Vedani^e

^a College of Materials Science and Engineering, Taiyuan University of Technology, Taiyuan 030024, China

^b Institute for Advanced Studies in Precision Materials, Yantai University, Yantai 264005, China

^c School of Metallurgy and Material Engineering, Chongqing University of Science and Technology, Chongqing, 401331, China

^d Magnesium Technology Innovation Center, School of Materials Science and Engineering, Seoul National University, 1 Gwanak-ro, Gwanak-gu, Seoul, 08826, South Korea

^e Department of Mechanical Engineering, Politecnico di Milano, 20156 Milan, Italy

ARTICLE INFO

Article history:

Received 28 June 2020

Accepted 2 September 2020

Available online xxx

Keywords:

Magnesium

texture control

plasticity

low temperatures

ABSTRACT

Owing to the hexagonal close-packed (HCP) crystal structure of magnesium alloys, they are characterized by poor plasticity at low temperatures (below recrystallization temperature), which limits their application. Texture control has been proven to be an effective way to enhance the ductility, formability, processability, and so on. Various technologies, which can be classified as alloying elements, induced shear deformation, pre-twins, and recrystallization, have been developed to modify the basal texture. Based on these results, the general mechanisms of texture control in various recent methods are summarized. In addition, applications of Mg products via texture weakening below recrystallization temperatures are also reviewed. Finally, the current problems and the potential research directions on texture control are suggested.

© 2020 The Author(s). Published by Elsevier B.V. This is an open access article under the CC BY-NC-ND license (<http://creativecommons.org/licenses/by-nc-nd/4.0/>).

Lifei Wang, get his MSc. and Ph.D. degree in Materials Science and Engineer at National Engineering Research Center for Magnesium alloys from Chongqing University of China. Study as a joint-Ph.D in Polytechnic University of Milan, Italy and Post-doc in Seoul national university, South Korea. At present works as associate professor in Taiyuan University of

technology. The research field focused on the deformation of magnesium alloys.

Maurizio Vedani, get his MSc. And Ph.D degree in Polytechnic University of Milan of Italy. At present works as full professor in Polytechnic University of Milan. He serves the head of materials section and deputy director of Department of Mechanical in Polimi. Once he is the President of the "Physical metallurgy and materials science" technical Committee of the Italian Association for Metallurgy and President of the "Light Metals" Committee in the same association. The research field

* Corresponding author.

E-mail: wanglifei@tyut.edu.cn (L. Wang).

<https://doi.org/10.1016/j.jmrt.2020.09.002>

2238-7854/© 2020 The Author(s). Published by Elsevier B.V. This is an open access article under the CC BY-NC-ND license (<http://creativecommons.org/licenses/by-nc-nd/4.0/>).

involves the light weight metals (Al, Mg and so on) processing and the biomaterials.

Kwang Seon Shin, Ph.D graduate in Materials Science and Engineer from Northwestern university of United States of America. Works as assistant, associate Professor (with Tenure) (1983-1991) in Arizona State University, USA. At present he is the full professor in Seoul National University of south Korea. Now he is the chairman of Korea Magnesium Technology Research Association and Director of Magnesium Technology Innovation Center in SNU. Once he serves as Co-Chair of the 6th International Conference on Magnesium Alloys (ICM6), the 10th International Conference on Magnesium Alloys and Their Applications (Mg 2015) and President of Korean Institute of Metals and Materials (>15,000 members).

1. Introduction

Owing to their high specific strength, stiffness, damping properties, and recyclability, magnesium (Mg) alloys have received considerable attention as the lightest structure metals owing to their electronic, automotive, aerospace, and biomedical applications [1,2]. However, because of their special hexagonal close-packed (HCP) structure, traditional wrought Mg alloys usually demonstrate low strength and plasticity (ductility, formability and processability etc.). The poor ductility of Mg alloys at room temperature has restricted their application because of cost-prohibitive processing at high temperatures (300–450 °C) [3,4]. Thus, investigations on improving the properties of Mg alloys at lower temperatures, especially the low recrystallization temperature, are urgently required to promote the industrial application of Mg alloys.

Magnesium alloys are usually fabricated as sheets, bars, wires, or tubes by rolling, extrusion, drawing, etc., and then used in forming Mg alloy sections. However, a deformation basal texture is generated [5–7]. The emergence of basal texture leads to a polar deformation mechanism, which has a significant effect on the properties of the alloy. It is well-known that slip systems in single Mg crystals include the $\langle 11\text{-}20 \rangle \{0001\}$, $\langle 11\text{-}20 \rangle \{10\text{-}10\}$, $\langle 11\text{-}20 \rangle \{10\text{-}10\}$ $\langle a \rangle$ slips, and $\langle a + c \rangle$ slips along the $\langle 11\text{-}23 \rangle$ direction on the $\{10\text{-}11\}$, $\{11\text{-}21\}$, $\{10\text{-}12\}$, and $\{11\text{-}22\}$ planes. However, the critical resolved shear stress (CRSS) of various slips is much different [8–11]. The CRSS of basal $\langle a \rangle$ slip, prismatic $\langle a \rangle$ slip, pyramidal $\langle a + c \rangle$ slip are approximately 0.5 MPa, 78 MPa, and 139 MPa at room temperature, respectively [12–14]. Therefore, non-basal slip is not easily activated. Twinning is another important deformation mechanism, and includes variants such as $\langle 1\text{-}210 \rangle \{10\text{-}12\}$ tensile twinning, $\langle 1\text{-}210 \rangle \{10\text{-}11\}$ and $\langle 1\text{-}210 \rangle \{10\text{-}13\}$ compressive twinning as well as double twinning. However, the CRSS of tensile twinning is much smaller, at only 2–3 MPa, while that for compressive twinning is 76–153 MPa [13,15,16]. Thus, basal slips and tensile twinning are the easiest to start during deformation. Usually, basal $\langle a \rangle$ slip is activated first, then $\{10\text{-}12\}$ tensile twinning starts when the basal slip is restrained. This is also the main determining factor in the generation of a strong basal texture on Mg alloys.

For magnesium alloys with a strong basal texture, the Schmid factor (SF) of basal $\langle a \rangle$ slip systems is much smaller when the tensile loading is along the rolling or extrusion

direction at room temperature, and the orientation of grains tends to be hard [17,18]. Additionally, prismatic $\langle a \rangle$ and pyramidal $\langle a + c \rangle$ slip cannot start at lower temperatures. Thus, the dislocations will be piled up and the motion is restrained, which results in a smaller fracture elongation [19,20]. For formability, texture also plays an important role. It is well known that the width strain is coordinated by a prismatic $\langle a \rangle$ slip, while the thickness strain is coordinated by pyramidal $\langle a + c \rangle$ slip during plane deformation on a magnesium alloy sheet with a strong basal texture [21–24]. However, non-basal slip cannot be activated so that the thickness deformation is no longer coordinated. The Mg alloy sheet undergoes severe thinning resulting in poor formability. When the basal texture is weakened, the orientation of grains rotates away from the normal direction (ND), which is favored for the activation of basal slip [25,26]. Thickness deformation, which results in the improvement of stretch formability, will be accommodated by basal slips. Therefore, texture control is an effective way to enhance the properties of magnesium alloys. In this review paper, various latest technologies for texture control at lower temperature blew recrystallization (especially below 423 K) are summarized, and some directions for further research are proposed.

2. Methods of texture control

In general, the c/a ratio is 1.622 for pure Mg, and the basal $\langle a \rangle$ slip along the $\langle 11\text{-}20 \rangle$ direction is much easier to start [27,28]. Thus, most grains are laid on the basal plane. Usually, a strong fiber basal texture is generated after extrusion, and a plane basal texture is achieved after rolling. The intensity of the basal texture is affected by the process parameters such as the deformation temperature and speed [29,30]. A strong basal texture is not favored by the activation of basal slip, which results in the poor plasticity of Mg alloys at low temperatures. In order to control the strong basal texture, the orientation of grains should be rotated, or other slip systems (non-basal slip) can be enhanced. Many methods for texture control have been developed based on this idea.

2.1. Addition of Elements

Adding elements into magnesium alloys is a typical and effective way to change the texture characteristics and weaken the basal texture. Recrystallization is an important factor that can alter the texture. After micro-alloying, the dynamic recrystallization (DRX) modes, that is, continuous DRX (CDRX) and discontinuous DRX (DDRX), are different during hot rolling or extrusion. The well-known dynamic recrystallization mechanisms mainly include particle stimulated nucleation (PSN), shear band nucleation, strain bulging nucleation, twins induced nucleation, and solutes driven effect [31,32]. Different recrystallization mechanisms may contribute to different new textures. The c/a ratio can also be changed due to the size differences of the atoms of the element within the Mg matrix. Therefore, the relative activation of slip systems during deformation is also responsible for the texture evolution. Based on the characteristics of various elements, they can be divided

into rare earth (RE) and non-RE element additions. These are reviewed in this section.

2.1.1. Rare earth elements

For pure Mg, the texture formation mainly results from the activation of tensile twinning and basal $\langle a \rangle$ slip due to the low CRSS. During hot extrusion or rolling, the basal $\langle a \rangle$ slip starts to coordinate deformation, and the basal pole rotates in the normal direction (ND). The strain bulging nucleation of DRX behavior occurs during hot deformation. However, it is reported that the orientation of new DRX grains induced by strain bulging nucleation will follow the parent grains during hot extrusion [33]. Thus, a basal texture is usually achieved in pure Mg. However, the deformation mode and DRX mechanisms begin to change after the addition of RE elements. Liu et al. [34] and Stanford [35] found that a special double-split texture was obtained in extruded Mg alloys after micro-alloying rare earth elements Y, Ce, Gd, and La into Mg-1.5Zn and pure Mg alloys, respectively. The special texture component was named rare earth (RE) texture. The intensity of the split (0001) basal texture was reduced as the concentration decreased. This means that these RE elements have similar functions in the formation of this type of split texture. It is suggested that the activation of slip systems and the alternative dynamic recrystallization (DRX) mechanisms are responsible for the formation of the relative textures [33,34].

For Y element additions, Kula et al. [36] indicated that the strong basal component disappeared gradually and a broader spread of basal poles around ND was observed on rolled Mg-Y binary alloys as the low concentration of Y increased to 0.82 %, as shown in Fig. 1(a). Shi et al. [37] found that the split RE-texture emerged when the high concentration of Y increased from 1% to 5%; meanwhile, a sharp basal texture was observed in pure Mg, as shown in Fig. 1(b). It was concluded that the basal texture could be weakened by the addition of Y elements, especially at high concentrations. This was related to the activity of non-basal slips and recrystallization behaviors. Due to the Y additions, the slip systems are strengthened, most the $\langle c + a \rangle$ slip system, followed by pyramidal I, prismatic, twinning and basal systems. All slip systems exhibit monotonic increase of CRSS with Y concentration, but at different rates. As previously stated, there are several factors that induce the nucleation of DRX in Mg alloys; for example, particle stimulated nucleation (PSN), shear band nucleation, and solar-driven effect. However, the shear bands could not be found in Mg-Y alloys. Thus, particle stimulated nucleation (PSN) or solar-driven effect may play an important role. In particular, the solar-driven effect, which dominated texture weakening, was because no precipitation occurred when the concentration of Y was lower than 1% in Mg-Y alloys. Furthermore, the texture was also associated with solute segregation. If the concentration of elements was too low and not enough to induce solute segregation, the texture weakening effect was not obvious. However, the effect was reduced when the concentration was too high to form precipitates. Because of solute segregation, non-basal slip was enhanced in the rich-solute regions, and caused uniform deformation so that strain induced DRX nucleation occurred easily and the basal texture was weakened. Besides, the precipitates formed with high Y concentration which can act as obstacles to retard the motion

of grain boundaries so that suppress the growth process of recrystallization. Both the nucleation and grain growth suppressing play an effect to increase the range of orientations that between the nucleated and deformed grains and the weakened basal texture is obtained.

Wu et al. [38] also reported that the c/a axis ratio of pure Mg decreased from 1.624 to 1.6222 and 1.6195 when 5 wt.% and 10 wt.% Y elements dissolved into the matrix in solution state. The stacking fault energy (SFE) on the basal and pyramidal planes decreased; therefore, the CRSS of pyramidal $\langle a + c \rangle$ slip was obviously reduced. In addition, the twins could be found in pure Mg; but the mixed deformation modes involving twinning and non-basal slip with low yttrium content (0.23 wt.%Y and 0.84 wt.%Y) alloys did not appear in the microstructure in Mg-2.71 wt.%Y alloys. This means that the activity of non-basal slip modes could be enhanced by increasing the Y element concentrations, so that the split RE texture was enhanced. Agnew et al. [39] also indicated that the c/a ratio was reduced after adding Y elements to pure magnesium. Non-basal $\langle a + c \rangle$ slip systems were activated, which resulted in the tendency of RD-split basal texture during rolling. Sandlobes et al. [40] reported that the stacking fault energy (SFE) on basal and pyramidal planes was reduced probably after adding Y elements, which led to the activation of $\langle a + c \rangle$ slip. Thus, a softening split texture after recrystallization is generated during hot rolling. In addition, it was found that the RE texture was generated only after a critical concentration threshold was reached following the additions [41]. Stanford [35] reported that the texture randomization happened after adding 0.04 at. % Y and became highly effective at 0.17 at. % Y. The nucleation sites for RE-textured nuclei were at the Y addition pots, and the growth preference was altered by changing the characteristics of grain boundary (GB) mobility during recrystallization. However, weakening basal texture by Y elements may be not much more effective due to its smaller atomic radius (close to Mg).

For the addition of Ce elements, a similar RE-texture was obtained in an extruded Mg-0.5% Ce magnesium rod, where most of the grains were in a non-basal orientation [42], as shown in Fig. 2. This was consistent with several studies. This means that the RE element, Ce, also plays a role similar to the addition of Y, of modifying the basal texture of Mg alloys. Masoumi et al. [43] suggested that the weakening of basal texture by Ce elements was related to the solid solubility of Ce in Mg and the stacking fault energy, which were not because of the change in the c/a ratio. After Ce addition, solute atoms preferentially segregate to the stacking faults contained in extended dislocations. As the amount of solute within the stacking faults increases, it lowers the stacking-fault energy and increases the separation of the partial dislocations. Not only the basal slip, but also more non-basal slips were promoted during the plastic deformation of the Mg-Ce alloys. Therefore, it can be concluded that the stacking fault energy of Mg is affected by the Ce addition and the anisotropy of CRSS for different slip systems is reduced. As a result, prismatic $\langle a \rangle$ slip along with basal slip has been activated more. And the basal texture is weakened obviously. Chino et al. [44] also indicated that the obtained double-peak RE texture on Mg-0.2 – wt.% Ce alloys after hot rolling at 400 °C was not due to the reduction in the c/a ratio. The c/a ratio did not

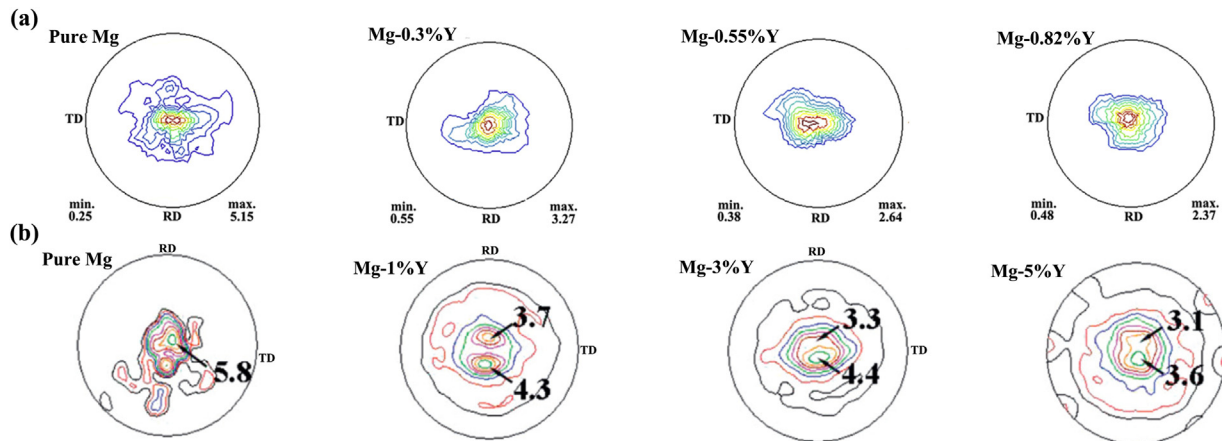


Fig. 1 – The texture evolution in various amounts of Y element added Mg alloys: (a) low concentration of Mg-Y binary alloys after cold rolling [36], (b) high concentration of Mg-Y alloys after hot rolling [37].

(0001) pole figures

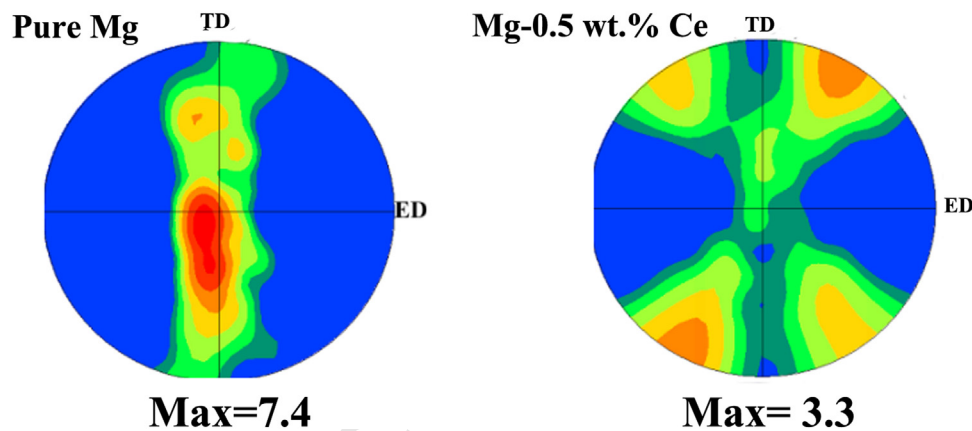


Fig. 2 – Texture evolution of Ce element added Mg alloys: (a) pure Mg, (b) Mg-0.5% Ce alloy after extrusion [42].

272 change significantly after Ce addition; however, the SFE value
 273 increased, which was beneficial for the activation of non-
 274 basal $\langle a \rangle$ and $\langle a + c \rangle$ slips. In addition, CDRX is promoted by
 275 the PSN mechanism, which also results in the weakening of
 276 the basal texture, especially at high concentrations [45,46]. At
 277 higher concentrations, precipitates adopt a string-like mor-
 278 phology (Fig. 7) which significantly reduces availability of sites
 279 where more grain orientations could nucleate. However, the
 280 texture weakening induced by PSN of recrystallization is lim-
 281 ited because of the solid small solubility of added elements
 282 (Ce). However, the effect of Ce on the stacking fault energy
 283 of Mg is still unclear which is required to be studied fur-
 284 ther.

285 For the addition of Gd and Nd, the RE-texture weakening
 286 effects are much more distinct, as shown in Fig. 3. Wu et al.
 287 [47] and Yan et al. [48] suggested the formation of a TD split RE
 288 texture in Mg-1Zn-x(1.0 wt.%, 2.0 wt.%) Gd alloys and Mg-2Zn-
 289 x (0.1 wt.%, 0.3 wt.%, 0.7 wt.%) Gd alloys was because of the
 290 activation of non-basal slip and recrystallization behaviors.
 291 Stanford et al. [49] reported that the RE-texture was enhanced
 292 with a higher concentration of Gd elements, as shown in
 293 Fig. 3. The PSN of recrystallization has been cited as a texture-

294 randomizing mechanism. Wu et al. [50] indicated that a large
 295 number of secondary twins and shear bands formed during
 296 the hot rolling of Mg-1Gd sheets, served as nucleation sites
 297 for recrystallization. The recrystallized grains at the shear
 298 bands in the Mg-1Gd alloy promoted a dispersive orienta-
 299 tion. The activity of pyramidal $\langle a + c \rangle$ slip was enhanced
 300 at the same time. The preferred growth of $\langle 11 - 20 \rangle$ grains
 301 was inhibited by Gd solute segregation at the grain bound-
 302 ary, which resulted in a double peak texture in the Mg-1Gd
 303 alloy sheet after annealing. However, the RE-texture trends to
 304 combine together in the (0001) basal pole when the concen-
 305 tration of Gd exceeds 4% wt. %, as shown in Fig. 3(b). This
 306 may be related to the segregation of Gd atoms at GBs, where
 307 the intergranular precipitations are formed so that the effect
 308 of Gd solutes or the random orientations of grain growth is
 309 restrained. The more random orientations of DRX grains in
 310 Mg-Gd alloys are attributed to the nucleation stage. Therefore,
 311 the concentration of Gd elements during addition should be
 312 considered critically. Yan et al. [48] also found that shear bands
 313 emerged in grains with c-axis parallel to the ND of Mg-2.0%
 314 Zn-0.8% Gd (wt.%) alloy sheets during hot rolling. Continu-
 315 ous dynamic recrystallization behaviors occurred around as

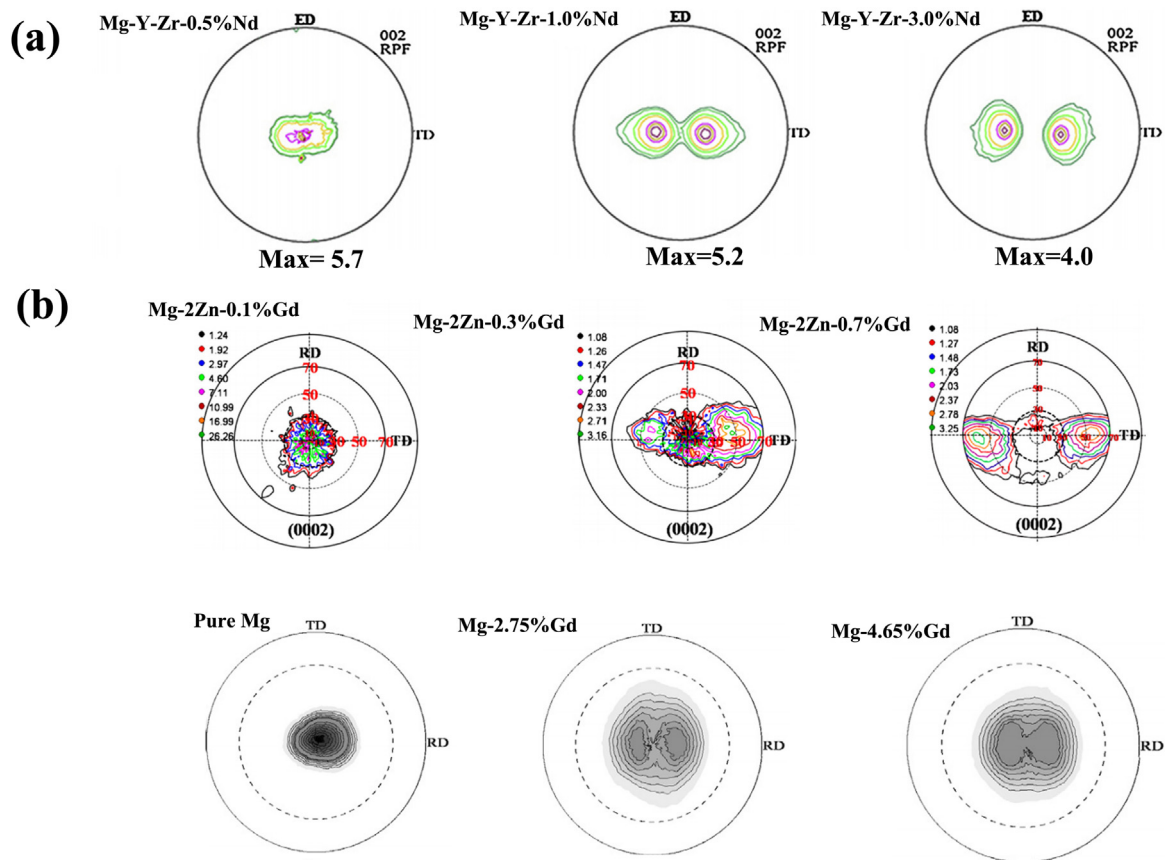


Fig. 3 – Texture evolution of Nd and Gd element added Mg alloys: (a) various concentration of Nd element added Mg-5.0Y-0.5Zr-xNd alloys [51], (b) various concentration of Gd element added Mg-Gd alloys [48,49].

well as inside the shear bands. EBSD analyses showed that the recrystallized new grains in the shear bands exhibited a “tilted” basal texture with the c-axis inclined $\pm 20^\circ$ from ND towards RD. Nd elements shows a very low solubility limit in Mg alloys, which expresses an excellent impact to weaken the basal texture even the concentration small as 0.04 at. %. Xu et al. [51] reported that the DRX was promoted by the particle-stimulated nucleation (PSN) and the PSN was the main mechanism for weakening the texture in Mg-5.0Y-0.5Zr-Nd alloys during hot extrusion. The nucleation of dynamic recrystallization and the volume fraction of recrystallized grains were promoted obviously after addition Nd from 0 wt. % to 2.63 wt. %. The particle deformation zones (PDZ) was formed close to the Mg-Nd phase which promoted the DRX nucleation. Besides, the Mg-Nd particles pinned the grain boundaries and reduced the movement which restrained the grain growth. These mechanisms caused the weakness of basal texture in the extruded alloys with Nd addition. Hantzsche et al. [52] and Hadorn et al. [53] also indicated that the RE-texture by micro-Nd alloys is connected to the solubility of the dissolved solid. Thus, the recrystallization behaviors, especially PSN mechanisms are much more important during texture control in Mg-Gd and Mg-Nd alloys.

For the addition of La and Sr elements, the basal texture could be also modified via DRX. However, more literatures could not be found which should be investigated further. Zen-

gin et al. [54] suggested that the texture weakening by La additions was because of PSN mechanism and solute atoms. After La addition into ZK60 Mg alloy, Mg-Zn-La particles were broken to pieces with the size larger than $1 \mu\text{m}$ which could set as the nucleation site for DRX during hot extrusion. The number of particles and the fraction of DRXed grains increased as the concentration increasing, which resulted in the texture weakening. The solute segregation of La atoms at grain boundaries should be also considered. For Sr element, Sadeghi et al. [55] recommended that the final texture of AZ31+Sr alloys during hot extrusion was affected by various DRX mechanisms. At low temperatures and low level of Sr addition, DRX induced by the grain boundary bulging was activated. In contrast, at high temperature and high level of Sr addition, PSN mechanism became much more significant. As shown in Fig. 4, the basal texture and intensity reduced after Sr and La addition. All in all, the formation of RE-texture was related to various DRX mechanisms and the enhanced activity of non-basal slip, like prismatic $\langle a \rangle$ slips and pyramidal $\langle a+c \rangle$ slips. The differences of atomic radius and the solubility limit between the RE elements and Mg matrix affect the effectivities. And the concentration of various additions plays a majority role how the basal texture weakens. However, the cost of RE elements is much more expensive. The low cost elements additions should be considered which has the similar functions to form the RE-texture.

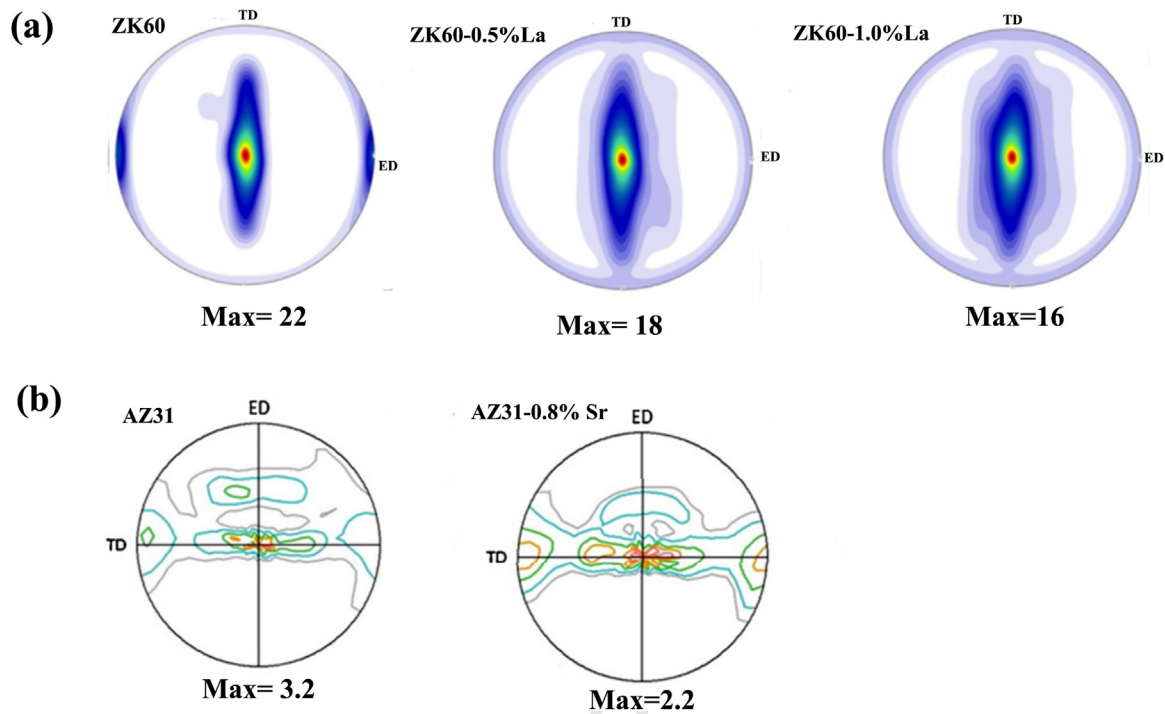


Fig. 4 – Texture evolution of La and Sr element added Mg alloys: (a) various La elements added ZK60 alloys [54], (b) various Sr added AZ31 alloys [55].

2.1.2. Non-RE elements

Not only do rare earth elements perform the function of texture weakening, but also some non-RE elements can promote the split double peak RE-texture. Wang et al. [56] indicated that a double peak TD-split RE texture emerged during hot extrusion after adding Zn into the Mg-0.2Ca-0.2Ce-x (0.5 wt.%, 1.0 wt.%, 1.5 wt.%, 2.0 wt.%) Zn alloys. The RE-texture tilted the basal poles 25° – 35° from the normal direction (ND) towards the extrusion direction (ED). The intensity of the basal texture gradually decreased with increasing concentration of zinc elements, as shown in Fig. 5(a). Zhang et al. [57] reported that the texture was similar to those alloys containing RE elements in which the basal texture was weakened by adding calcium (Ca) elements. The $\{11-20\}$ plane of the gains was parallel to the extrusion direction and became a strong second texture, as shown in Fig. 5(b). A similar phenomenon is also observed after adding Li element to AZ31 Mg extruded alloys [58], as shown in Fig. 5(c). The reasons for the formation of the split RE-like texture are similar to the additions of rare earth elements. After adding zinc and calcium, the c/a ratio did not change significantly; however, the stacking fault energy (γ_{US}) increased. It was reported that the value of γ_{US} (basal) of the Mg-Zn-Ca model was larger than that of the Mg-Ca model; while γ_{US} (basal) and γ_{US} (prism) of Mg-Zn-Ca model was almost equal [59]. This means that the activation of non-basal prismatic $\langle a \rangle$ slip systems could be enhanced by the addition of Zn and Ca, which played a function similar to that of Y, Ce, Gd etc. The solid solubility and PSN mechanism induced by DRX were also considered to be a response to texture weakening. However, a low concentration of 0.2% Ca or 0.5% Zn already resulted in a large difference in texture compared to the initial Mg alloys, so that Zhang et al. did not

attribute texture modification to the solid solubility. Thus, the PSN mechanism of DRX was a response to texture weakening. For the Li element, similar reasons were expressed for texture evolution.

Overall, based on the texture weakening mechanisms above, the addition of alloy elements to form the double peak TD split texture seems to be related to the c/a ratio and the stacking fault energy of Mg alloys. Owing to the addition of alloy elements, lattice distortion occurs such that the c/a ratio reduces and the stacking fault energy increases, which favors the activation of non-basal $\langle a \rangle$ and $\langle a+c \rangle$ slips. Thus, the non-basal texture will be enhanced and the basal texture component is weakened. Dynamic recrystallization also plays a significant role in the orientation generation of new recrystallized grains after hot extrusion or rolling. Solute-driven effects and PSN-induced DRX recrystallizations are much more important. However, there is a critical concentration to produce the RE-texture by micro-alloying. With a high concentration of alloying elements, the particles not only promote the nucleation, but also restrain the DRX grain growth which does benefit to the texture weakening at the same time. This is appropriate not only for rare earth but also for other elements such as Ca, Zn, and Li. Therefore, promoting non-basal slips or DRX behaviors is a way for potentially modifying the basal texture during alloy design. The inclined degree and direction of the basal pole also needs to be precisely controlled. It is known that the atomic radii of various elements are different, especially between RE-elements or non-RE elements and the Mg matrix, which results in differences in the induced lattice distortion. There are obvious changes on the c/a ratio and stacking fault energy, which enhance non-basal slips. However, it should be noted that for some elements such as Li or

(0002) pole figures

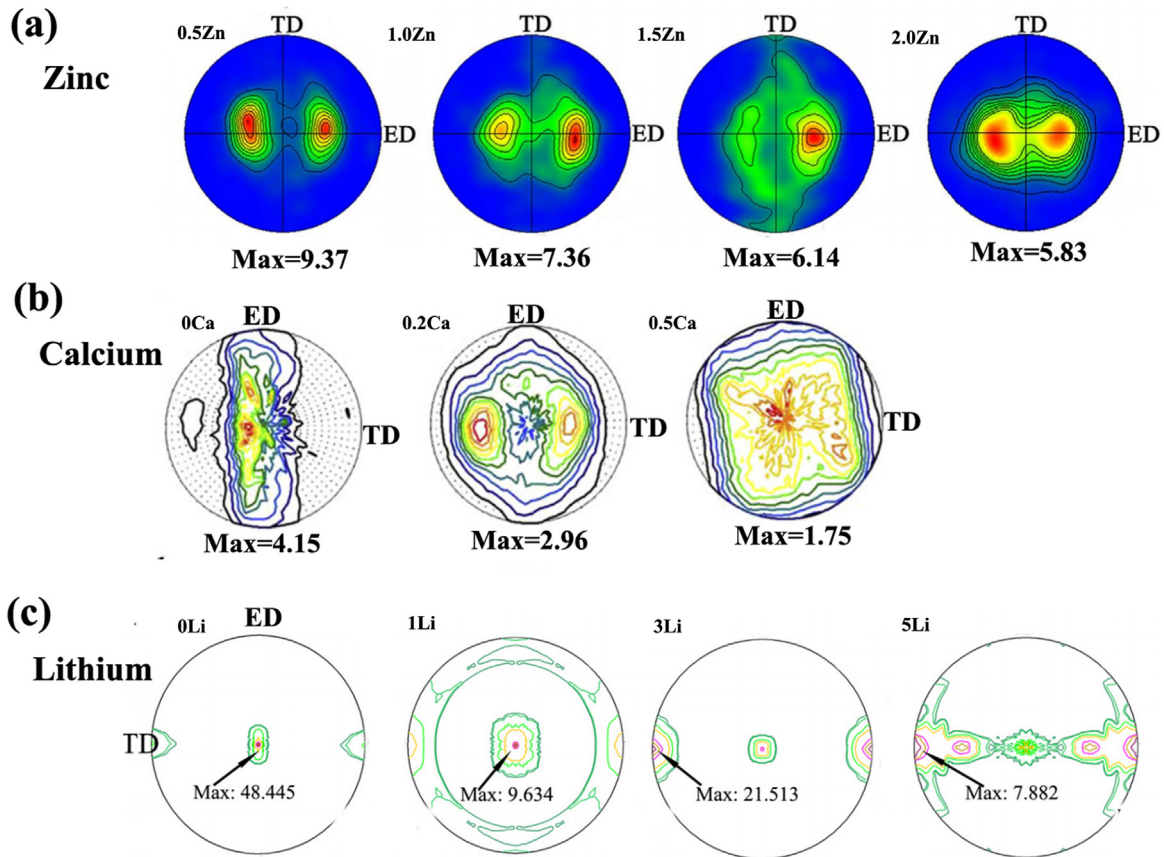


Fig. 5 – Texture evolution of Zn, Ca and Li elements added Mg alloys: (a) various Zn element added Mg-0.2Ca-0.2Ce-xZn alloys [56], (b) various Ca element added ZK60 alloys [57], (c) various Li element added AZ31 alloys [58].

Zn, the atomic radius is similar to that of Mg, and the c/a ratio does not change significantly. The RE-texture emerges and the basal texture can be weakened greatly as well. There may be different reasons for this. Therefore, the general mechanisms for obtaining a weaker basal texture modification regardless of whether there are RE elements or not during alloy design, are still unreported and should be investigated in the future. The effect of alloy elements on the stack fault should be studied deeply also.

2.2. Induced shear deformation

It is well known that the orientation of grains will rotate during deformation. Thus, texture can be controlled by a special deforming process, namely induced shear deformation. Induced shear deformation promotes the activity of non-basal $\langle a \rangle$ and $\langle a + c \rangle$ dislocations as well as twinning, so that the orientation of grains rotates away from the basal plane. After the induced shear deformation, a new texture component is generated or the intensity of the basal pole is decreased. For example, Agnew et al. [60] introduced shear deformation by the equal channel angular pressing (ECAP) process on AZ31 Mg alloy extrusion bars with an internal angle

of $\phi 90^\circ$ at 200°C . The viscoplastic self-consistent (VPSC) polycrystal modeling on texture evolution was also conducted for comparison. This indicated that the texture evolution induced by ECAP was related to the relative activity of basal $\langle a \rangle$ non-basal $\langle a \rangle$ and non-basal $\langle a + c \rangle$. The $\langle 0001 \rangle$ fiber texture tilted at $\sim 20^\circ$ was vertical to the extrusion direction after one single pass, and the tilted texture was enhanced after the multipass ECAP process. This was due to the activity of non-basal prismatic $\langle a \rangle$ slip and pyramidal $\langle a + c \rangle$ slip; however, the basal $\langle a \rangle$ slip still dominated the deformation while the non-basal slip accommodated the deformation by no more than $\sim 20\%$ during the single-pass ECAP. After the second pass, the activity of non-basal $\langle a \rangle$ and $\langle a + c \rangle$ slip was promoted, which resulted in the enhancement of the tilted texture rotating towards the (10-10) plane. Additionally, different alloys exhibited different deformation mechanisms; for instance, AZ alloys appear to exhibit balanced secondary slip of non-basal $\langle a \rangle$ slip and $\langle a + c \rangle$ dislocations, whereas ZK60 and WE43 appear to favor non-basal $\langle a + c \rangle$ slip during ECAP. The twinning and recrystallization also play an important role in texture evolution. Especially in high-alloy RE-Mg alloys, the shear bands, particles, and twins within the matrix may provide recrystallization nucleation sites that

476 promote grain orientation rotation during shear deformation.
477 This mechanism is similar to the elements alloying mecha-
478 nism described in the last sub-section. To focus on the effect
479 of induced shear deformation, only the AZ31 alloys without
480 dissolved precipitation are discussed in this section. Addition-
481 ally, the role of twinning in texture control will be discussed
482 in the following section. Particularly, {10-12} tensile twinning
483 is a very important deformation mechanism at low tempera-
484 tures, which rotates the grains approximately 86.3° away from
485 the basal plane and is less activated at elevated tempera-
486 tures.

487 The technologies for texture control by induced shear
488 deformation have been developed by many researchers. The
489 typical method is ECAP. During ECAP, the cross-sectional
490 dimension of the sample is not changed so that gains can be
491 refined easily by several extrusion passes. Shear deformation
492 is introduced at the channel corner [61–63]. However, the large
493 size of Mg alloys cannot be obtained through ECAP or simi-
494 lar processes owing to the limitations of the devices. For the
495 application of texture-controlled Mg alloys in industries, new
496 methods have been recently developed for the production of
497 large billets, tubes, and sheets.

498 For round or bloom Mg alloy billets and tubes, most of
499 the reported processes are based on the combination of
500 the ECAP process and extrusion deformation. The cast Mg
501 alloys undergo extrusion deformation with several shear steps
502 directly, which is beneficial for the continuous production
503 of large billets. Li et al. [64] developed the continuous vari-
504 able cross-section direct extrusion (CVCDE) process, where the
505 changing shear strain is applied by several interim dies as
506 shown in Fig. 6(a). After carrying out CVCDE with 2 interim
507 dies at 350 °C on AZ31 Mg alloys, the {10-11} pyramidal plane
508 is gradually parallel to the normal direction (ND) owing to the
509 activity of non-basal $\langle a + c \rangle$ slips. Moreover, the basal texture
510 weakened as the interim dies increased. Besides, the angle
511 between the most of the basal surfaces of grains and the extru-
512 sion axis is more closer 45° as the temperature increases to
513 350 °C. The basal texture is weakened future. This is related to
514 the dynamic recrystallization behaviors during CVCDE, which
515 is mainly continuous dynamic recrystallization (CDRX). Due
516 to the local strain at the interim dies, the twins may occur
517 at beginning and the low angle grain boundaries (LAGBs) are
518 formed. Then the LAGBs transform to high angle grain bound-
519 aries (HAGBs) due to the CDRX as the deformation continues.
520 The orientation of grains rotates away from the basal plane to
521 the shear direction. As the temperature increasing, the DRX
522 is promoted more and the rotation angle is larger. However,
523 the small grains produced by dynamic recrystallization start
524 to grow up at higher temperature and the coarse grains appear
525 in the microstructure. Hu et al. [65] and Liu et al. [66] developed
526 a continuous extrusion shear process (ES) in which the shear
527 strain was introduced by a deformation similar to ECAP com-
528 bined with the extrusion stage, namely extrusion-shear (ES)
529 and direct extrusion and bending-shear (DEBS), respectively.
530 However, more channels were added, as shown in Fig. 6(b)
531 and (c). The equivalent strains during the whole ES process
532 decreased as the channel angle increases. For DEBS, it is simi-
533 lar with the CVCDE process. During the DEBS deformation, the
534 DRX plays an important role on the microstrue and texture
535 evolution. The {10-12} tensile twinning happens at the first

536 stage and the grains rotate away from the basal pole induced
537 by the twins. As the extrusion bending-shear deformation
538 continuing, the subgrains and LAGBs transform to HAGBs.
539 Besides, the non-basal slip systems are activated during the
540 bending-shear deformation which promotes the formation of
541 the non-basal texture. Thus, the basal texture is weakened
542 greatly. Above all, it can be seen that DRX plays an impor-
543 tant role on the basal texture weakening induced by shear
544 deformation. Based on this idea of combination, a texture-
545 controlled tube can also be fabricated. Faraji et al. [67] and
546 Hu et al. [68] added internal shear steps in the tube extrusion
547 dies, and the TES (tube extrusion shearing) process could be
548 conducted. In that way, the grains would be reduced and the
549 texture weakened simultaneously, as shown in Fig. 6(c) and (d),
550 respectively. These serious technologies can realize the tex-
551 ture weakening and grain refinement continuously, however,
552 a higher load is required usually owing to the larger strain. The
553 microstructure is not homogeneous and grains grow up when
554 the deformation temperature is high. Two step texture con-
555 trolling may be an effective way to solve the problem. During
556 the first deformation stage, the texture can be weakened by a
557 smaller strain then a larger strain can be processed smoothly
558 at a lower temperature.

559 However, extrusion combined with ECAP-similar process
560 deformations are mostly used for bulk forming, which is dif-
561 ficult for sheet forming. Researchers have also investigated
562 rolling with shear deformations to produce a thin sheet with
563 a large volume. Differential speed rolling (DSR) is a typical
564 process in which shear deformation can be introduced by
565 asymmetry deformation through different rotation speeds
566 for the upper and lower rolls. This intense shear strain in
567 the entire deformed part may be utilized for achieving a
568 fine-grained microstructure and texture control. Huang et al.
569 indicated that the basal pole of Mg alloy sheet tilted towards
570 the rolling direction after conducting DSR on AZ31 [69], AZ61
571 [70], AZ80 [71] magnesium alloy sheets. It was reported that
572 the weakening of the basal texture was related to RDRX espe-
573 cially after multiple passes at higher temperatures. The RDRX
574 tended to take place at high temperatures in materials in
575 which the grains were not favorably orientated to accommo-
576 dating the rolling strain. Shear deformation promoted RDRX.
577 In addition, the induced shear deformation had effects on
578 enlarging the fraction of high-angle grain boundaries and the
579 misorientation angle, which randomly contributes to the basal
580 texture [72]. On the other hand, the shear band and twins
581 might be generated in the near-surface region. These could
582 be nucleation sites during recrystallization, which lead to the
583 rotation of the grain orientation. The spread of the (0002) ori-
584 entation may be associated with the activation of prismatic
585 slips. Hamad et al. [73] indicated that the routes also had
586 important effects on the texture evolution during the DSR
587 process. The DRX behaviors were promoted by cross-shear
588 deformation. The new DRXed grains were oriented randomly
589 at the expense of (0001)//ND-oriented grains (basal-oriented
590 grains), which in turn led to a basal texture weakening, as
591 shown in Fig. 7 (a). Equal channel angular rolling (ECAR) is
592 another important process that has significant potential for
593 use in the production of large volumes of texture-controlled
594 Mg alloy sheets. During the process, a special sheet ECAP die
595 follows at the end of the rolling deformation, and the shear

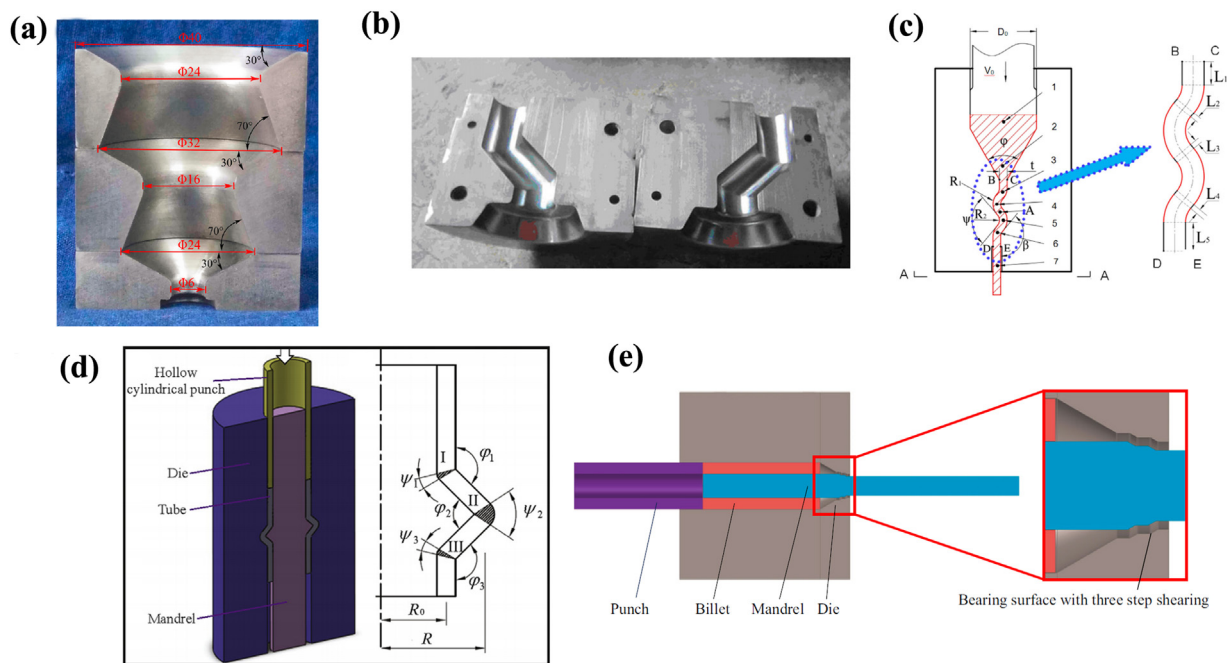


Fig. 6 – Various technologies to introduce the continuously shear deformation: (a) continuous variable cross-section direct extrusion (CVCDE) [64], (b) extrusion-shear (ES) [65], (c) direct extrusion and bending-shear deformation (DEBS) [66], (d) tubular channel angular pressing [67], (e) tube extrusion shearing [68].

596 strain is introduced. The texture-controlled mechanisms are
 597 similar to the ECAP process, which is related to the non-basal
 598 slip activity and dynamic recrystallization. Based on this, Song
 599 et al. [74] developed a new process for equal channel angular
 600 rolling with a continuous bending deformation (ECAR-CB) that
 601 has proven to be much more effective at weakening the basal
 602 texture than simple ECAR. This was not only because of the
 603 activity of non-basal slip, DRX, and the {10-12} tensile twins.
 604 The {10-12} tensile twins were activated in the inner layer
 605 under compressive stress. After annealing, the double-peak
 606 twinning texture was maintained, and the basal texture was
 607 weakened remarkably, as shown in Fig. 7(b). However, there is
 608 a gradient texture evolution through the sheet thickness. Like
 609 in DSR, the surface layer exhibits an obvious weakening basal
 610 texture; however, the intensity of (0002) pole is much higher
 611 in the middle layer. Besides, it is reported that the weakened
 612 double peak texture is not stable that needs to be investigated
 613 further. It expresses a similar phenomenon in ECAR-CB sam-
 614 ples. How to reduce the gradient microstructure and texture
 615 evolution is a potential direction in the future.

616 Recently, a new technology called asymmetric extrusion
 617 (ASE), was developed by Yang et al. The shear strain is induced
 618 not only by shear channel steps, but also through asymmet-
 619 ric velocity evolutions during extrusion [75–77]. This method
 620 is very simple and is similar to the conventional extrusion
 621 process. However, a large degree of asymmetric shear de-
 622 formation was introduced through the gap between the upper
 623 and lower surfaces in the ASE die equipped with a differ-
 624 ent parallel flow passage length, as shown in Fig. 8. The
 625 asymmetric flow velocity can be controlled by the length of
 626 extrusion passage. The simple shear enforces the near-surface
 627 microstructure to exhibit more dynamically recrystallized

628 grains having the c-axis tilted toward the extrusion direc-
 629 tion. The grains are favored for prismatic (a) slip than basal
 630 (a) slip during the ASE process. Therefore, the activation of
 631 prismatic (a) slip results in a rotation of the basal plane from
 632 the ED toward the imposed shear direction. The CE sheet
 633 developed a splitting of the pronounced basal texture after
 634 hot-extrusion. The (0002) basal texture intensity of the ASE
 635 samples in the top region decreased, as shown in Fig. 8(b).
 636 This study gives another perspective, which is that the shear de-
 637 formation can be introduced by materials flow control, not only
 638 by the different speed metal flow processes, but also by gra-
 639 dient deformation temperature or friction factors. It is more
 640 effective and convenient to obtain the texture weakened Mg
 641 alloy sheet. However, the gradient microstructure is also one
 642 problem which should be considered to reduce.

643 Besides extrusion and rolling with shear deformation,
 644 many other technologies such as bending processes have
 645 been developed simultaneously. Huo et al. [78] demonstrated
 646 that a fine-grained microstructure with an average grain size
 647 of $\sim 8 \mu\text{m}$ and a random basal texture of AZ31 Mg alloys
 648 was achieved by various cross-wavy bending routes. However,
 649 these bending routes can only be conducted at a high tem-
 650 perature of approximately 400°C due to the poor formability
 651 of magnesium alloys. Texture evolution is related to dynamic
 652 recrystallization (DRX) rather than shear deformation. The or-
 653 ientation of the new DRX grains is freshly generated. Thus, the
 654 texture controlling mechanism is complex and needs to be
 655 investigated further. Another bending process can be carried
 656 out at room temperature smoothly, and the texture is con-
 657 trolled well. Huang et al. [79–81] reported that the c-axis of
 658 grains tended to be inclined from the normal direction (ND)
 659 toward the rolling direction (RD) after repeated unidirectional

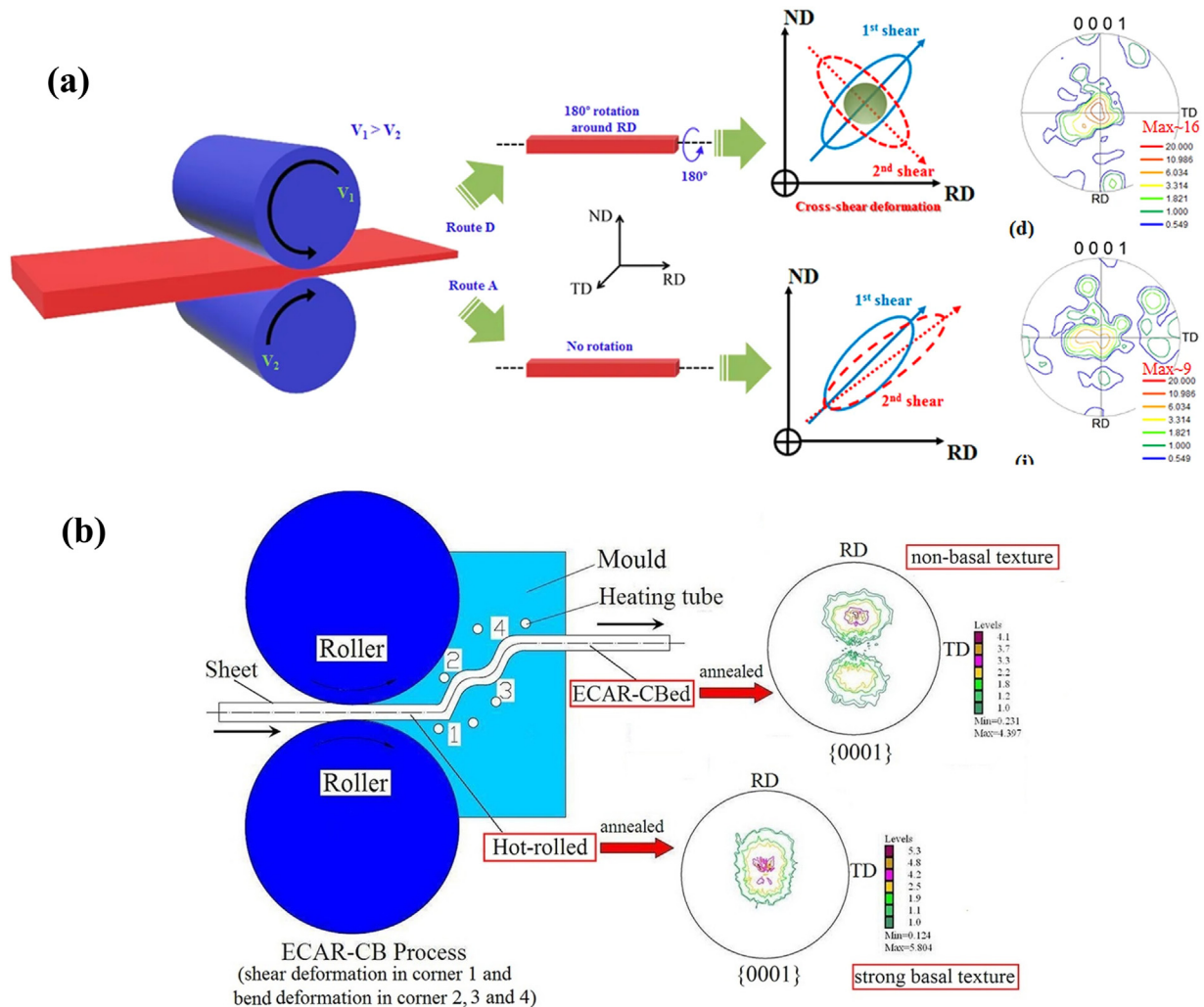


Fig. 7 – The schematic diagrams of rolling induced shear deformation: (a) various routes differential speed rolling (DSR) process [73], (b) equal channel angular rolling (ECAR) combined continuous bending deformation [74].

bending (RUB) process at room temperature. The basal texture components became more dispersed along the RD, and the intensity was greatly weakened, decreasing from 30.6 to 9.3 as shown in Fig. 9. This gives us guidance that the induced shear deformation at room temperature may be more effective during texture control.

Above all, induced shear strain can promote grains to rotate away from basal pole so that the basal texture is modified. The texture characteristic and intensity can be controlled by the shear path, the shear channel angle and so on, which is proven to be much more effective. However, almost current technologies are not easy to produce Mg alloy billets or sheet with large size, like typical ECAP. How to obtain larger texture-controlled Mg alloys continuously by induced shear deformation is significant for their application in industries. Developing new methods is necessary. Combining the induced shear strain during extrusion or rolling is a potential way to get the large size texture weakened Mg alloys, like DSR or CSE. The cast billets are suffering shear strain directly and the large-scale texture-controlled Mg alloys are achieved. As well known, Mg alloys are difficult to be deformed because of the crystal struc-

ture, and the deformation mechanisms are sensitive to the strain rate as well as temperature. The shear strain may be also induced by promoting asymmetry metal flow. Based on this idea, asymmetric extrusion (ASE) is effective to weaken the texture. Furthermore, the asymmetry metal flow may be induced by gradient deformation temperature or local friction factors. However, these series new SPD technology with shear deformation always results in a gradient microstructure and texture through the radial/thickness direction. How to promote the grain structure uniformly through the asymmetry gradient deformation should be considered. Besides, the grain growth at higher deformation temperature should be also avoided. A low temperature texture controlling method is need in the future study.

2.3. Pre-twinning and Recrystallization

{10-12} tensile twinning is an important deformation mode in Mg alloys, that rotates the grains 86.3° away from the basal plane [82]. For magnesium alloys, {10-12} tensile twinning is easily generated by pre-strain (<5%) owing to its lower CRSS

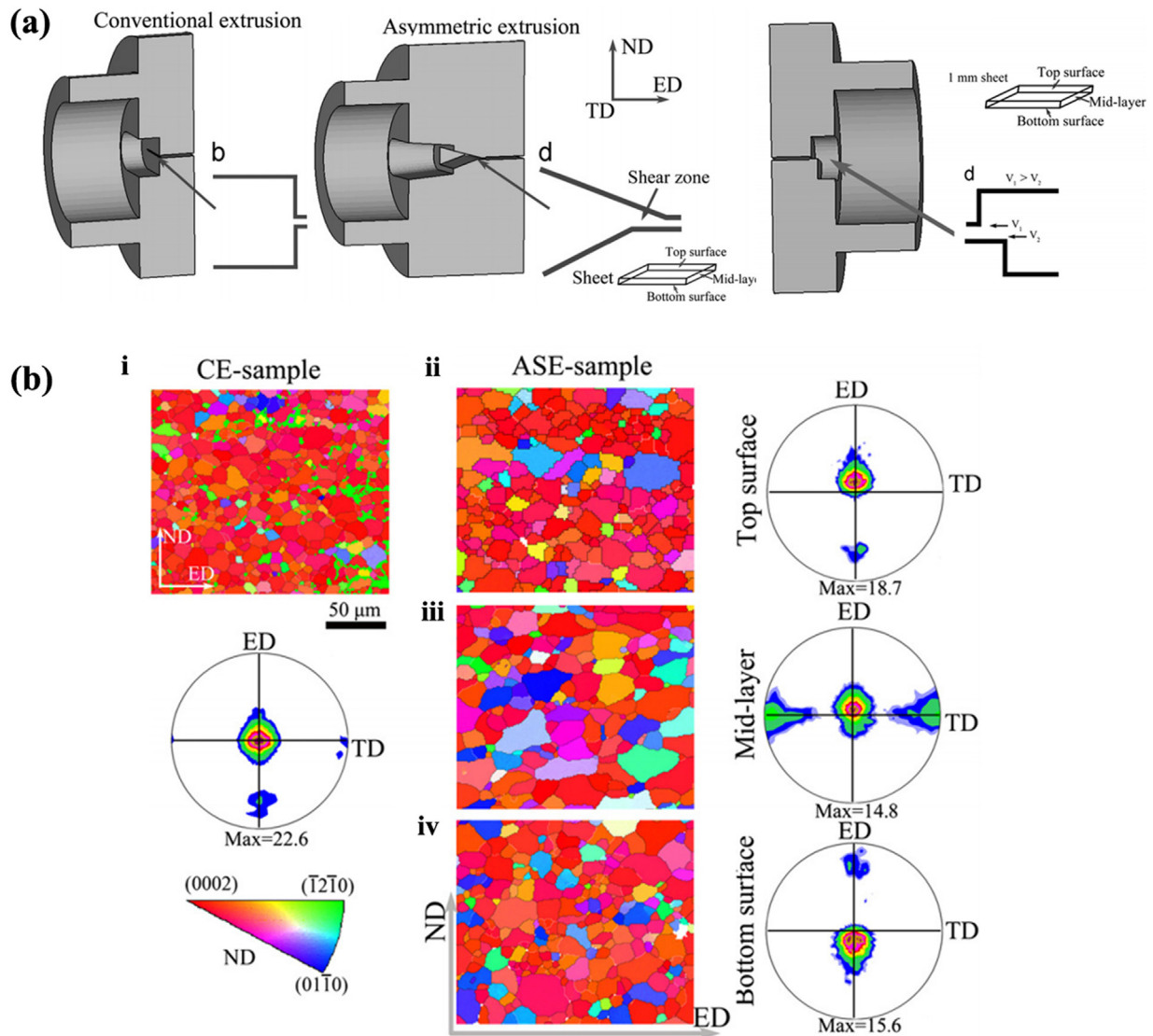


Fig. 8 – (a) Schematic sectional view of the conventional extrusion die, (b) (0002) pole figures and EBSD orientation maps of the CE sample (i), and the ASE sample at the top surface (ii), mid-layer (iii) and bottom surface (iv) [75,76].

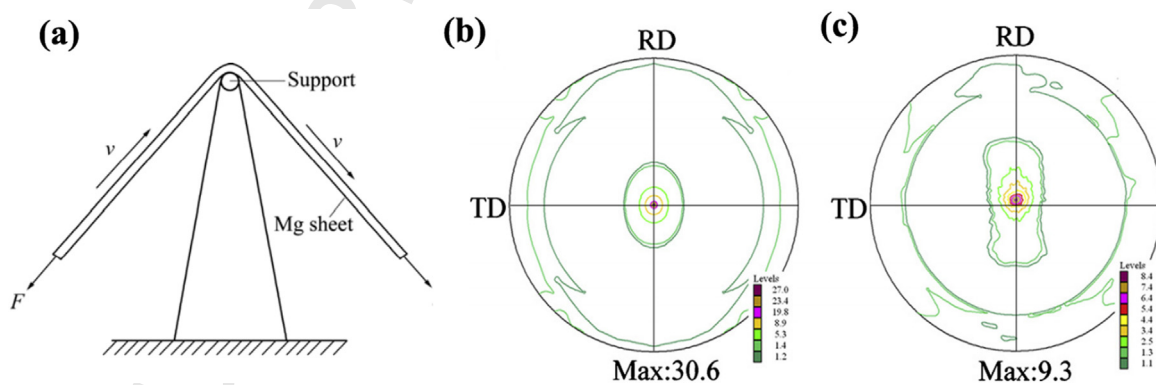


Fig. 9 – (a) Schematic illustration of apparatus for RUB, (0002) pole figures of (b) as-received sheet and (c) RUB processed sheet [79].

at room temperature [83]. However, twinning is a polar deformation mechanism that is activated only when the applied compressive load or tensile load is perpendicular or parallel to the c-axis of grains [84,85]. As the volume fraction of tensile twins increases, more grains rotate away from the basal pole and the texture component changes as well. Twinning lamellas can divide grains that also serve the function of grain refinement. Thus, pre-twinning can be another way to control texture.

Song et al. [86] conducted pre-cold rolling on AZ31 magnesium alloy thick sheets along the TD with various degrees of strain at room temperature. After annealing at 200 °C for 6 h, twinning lamellae were kept in the microstructure. Due to the {10-12} tensile twins, the grains rotate from ND to TD ~86° and a c-axis/TD texture was obtained. The intensity of the (0002) basal pole was greatly reduced compared to that of the as-rolled Mg alloy sheet. As the pre-strain degree increased from 3% to 5%, the volume fraction of twins increased and more grains were rotated to TD, the intensity of the basal texture were weakened more. Thus, the texture can be controlled to rotate the grain orientation by pre-induced twins. However, the twinning lamellas in one grain are parallel to each other and easy to grow, rather than nucleate, when the pre-strain degree is larger than 8%. Xin et al. [87] pre-compressed AZ31 magnesium alloy blocks along RD by strains of 1.8% and 6%, and then the samples were subjected to 8% recompression along the TD. Subsequent annealing was performed at 200 °C. After pre-compression along the RD for 1.8%, the (0002) poles of some grains rotated to RD, while both the (0002) poles rotated and unrotated during pre-compression inclined to TD. Similar results were obtained for a 6% pre-compression of specimens. The pole figure of the sample with only 8% compression along the TD was obtained, as shown in Fig. 10. This indicated that the twins had nearly completely nucleation under a compression strain of 2%, and grew under a strain of between 2% and 6%. At a strain level of 8%, most grains were nearly completely twinned and grown. In order to obtain more initial twins so that more grains rotate away from basal pole, the nucleation is better to be promoted and the grain growth is restrained. Therefore, the critical strain levels should be considered during introducing more initial twins at room temperature.

Almost all researches on the effects of induced {10-12} twins on texture are focused on thick plates or blocks. For a thin sheet, bending-buckling is much easier so that the pre-twinning process cannot be conducted from now on. Park et al. [88] pre-twined an AZ31 Mg alloy sheet with a thickness of 30 mm along the TD. Then, a thin sheet of 1 mm was cut from the sheet along the thickness direction. However, this is not convenient, and the microstructure gradient cannot be avoided during cutting from the block. Besides, a surface stress may be also introduced which has an effect on the initial twins. Thus, a new method for pre-induced twins on thin sheets is necessary, especially a uniform one. Wang et al. [89] and Kim et al. [90] made a try on this development. As shown in Fig. 11(a), a special device with side forces is provided by two splints, and the high-strength quenched Cr12 steel sheet with the same thickness as the Mg sheet is set as a pressing plate. Because the strength of steel is much higher than that of Mg alloy sheets, the deformation on the pressing plate can

be ignored. Thus, the clamping force ensures that the sheet avoids bending during precompression to induce initial {10-12} tensile twins. Similarly, the specimens in Kim's device are held by the clamping force and the anti-buckling force, which is much more complex. Though both two kinds of methods can pre-twins successfully on Mg alloy thin sheet with thickness of 1 mm, the dimension of the pre-twined samples are two small. The length or width is less than 50 mm, which limits its application during sequent forming. Therefore, new continuous and simple pre-twinning devices on Mg alloy thin sheets with larger scale should be developed in the future. Besides, previous studies on magnesium alloys have mainly focused on {10-12} tensile twins. It is well known that {10-11} compression twins rotate the grain orientation as well as the double twins, by approximately 38° or 56° et al. They may also be used to control the texture. However, these kind work are rarely reported which can be studied in subsequent investigations.

It is well known that slip and twinning play an important role in the deformation of magnesium alloys at room temperature. However, the microstructure continuously evolves into recrystallization during thermal mechanical processing. During recrystallisation behaviors, new grains are nucleated and grown arranging the orientation. It has been reported that the recrystallization texture is not only dependent on the orientation of the nuclei but also on the growth of the specific orientation [91]. The weakened recrystallization texture has been proposed to be related to particle-stimulated recrystallization, strain-induced recrystallization, and deformation twin-induced recrystallization [7,92]. Samman et al. [93] extruded Mg-1Zn-0.4Zr magnesium alloys and a modified version of the same alloy containing Nd-based rare earth mischmetal and Y at 400 °C. The results showed that the microstructure with the spheroidal particles inside the circled area was consistent with very fine grains ($d \sim 5 \mu\text{m}$), whereas the grain structure in the adjacent "particle-free" area (outside of the circle) is significantly coarser ($d \sim 40 \mu\text{m}$). Second-phase particles in the modified alloy provide additional nucleation sites for recrystallization and generate new orientations other than the deformed orientation. The effect of DRX nucleation on the texture evolution has been discussed in the previous section. Meanwhile, Zhang et al. [94] pre-stretched AZ31 magnesium alloy sheets at room temperature followed by annealing. The strain induced static recrystallization started and a critical strain of 5% emerged between grain nucleation and growth. Exceeding the critical strain, the speed of grain nucleation was faster than that of growth. Due to grain growth, the basal texture was weakened at the same time. The larger the grain size, the weaker the basal texture. According to Hall-petch relationship, the bigger of the grain size, the poor plasticity will be. However, it is opposite during plane deformation. The weakened basal texture plays more important role to reduce the anisotropy rather than grain growth which does help to improve the formability. This will be discussed in the following part.

Twins might also promote the recrystallization for Mg alloys. Xin et al. [95] reported that the stored energy accumulation within {10-12} tensile twinning boundaries was quite low. Thus, tensile twins could not act the site for recrystallization on AZ31 Mg alloys. While the strain induced recrystallization mechanism was dominated after pre-cold rolling and

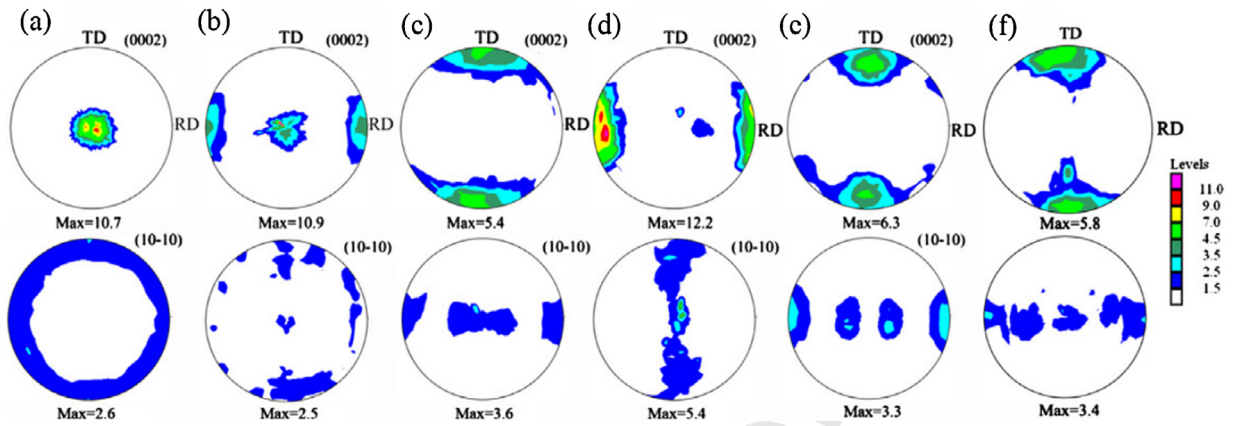


Fig. 10 – Pole figures of samples: (a) as-used material; (b) RD 1.8%; (c) RD 1.8% with 8% recompression along TD; (d) RD 6%; (e) RD 6% with 8% recompression along TD; (f) sample with 8% compression along TD [87].

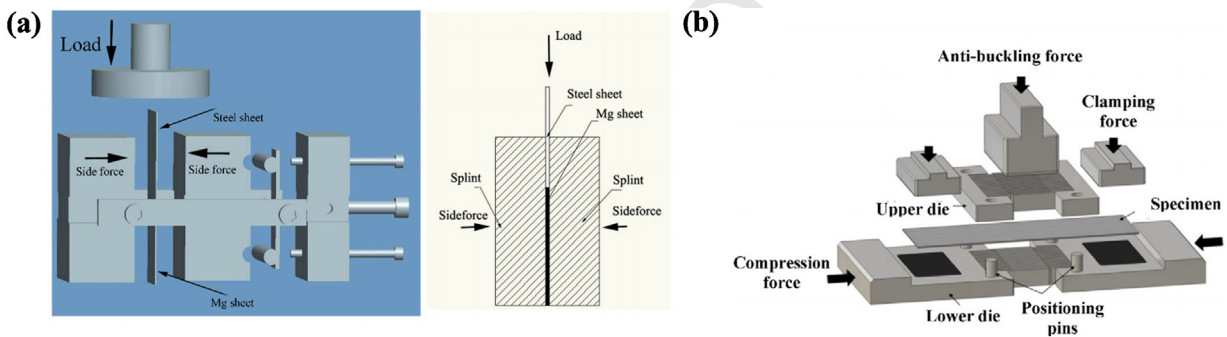


Fig. 11 – The schematic diagrams: (a) thin sheet compression device by wang et al. [89], (b) tension-compression machine by Kim et al. [90].

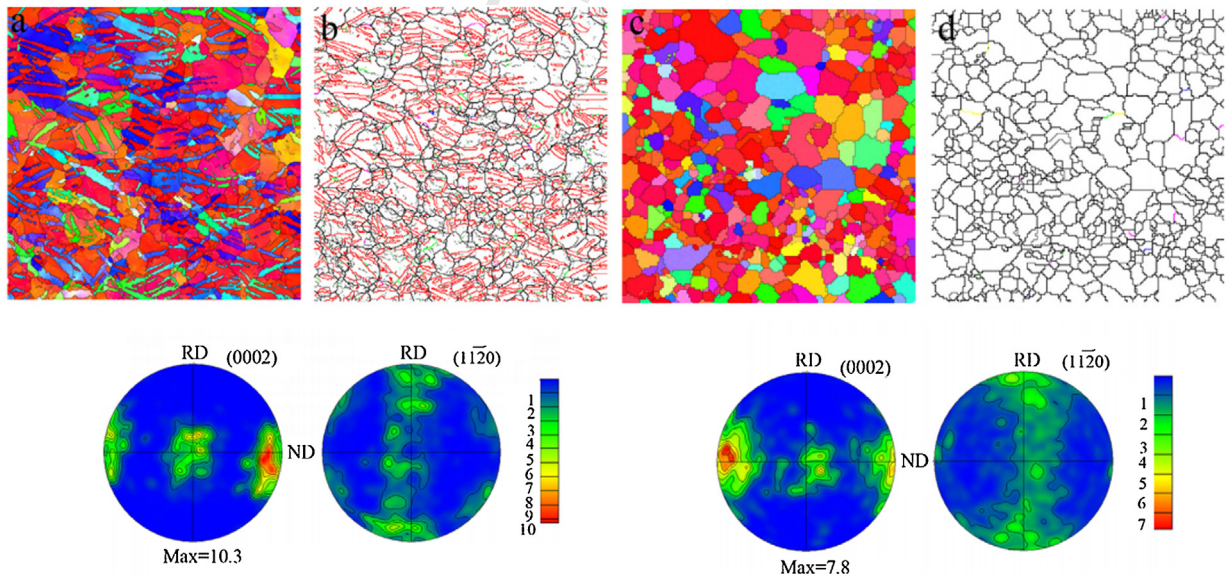


Fig. 12 – EBSD maps and (0002) pole figures of pre-twinned AZ31 Mg alloys: (a) before annealing, (b) after recrystallization annealing [95].

annealing. Thermally activated boundary migration (TABM) on {10-12} tensile twins extensively took place and the grains grew up at 300°C. By tracing the twins and new recrystallized grains, it was found that the orientation of grains at

grain boundaries was generally followed that of their neighboring parent grains, but spread moderately. Therefore, a TD closed orientation in recrystallized grains was obtained and the texture was weakened after annealing at 250°C for 1 h,

as shown in Fig. 12. Recrystallization induced by twin-twin intersections on tensile twins introduced another recrystallization mechanism. Yu et al. [96] indicated that the tensile twin-twin intersections contained many boundary dislocations. Therefore, the intersections could be regarded as the nucleation site for recrystallization. Cheng et al. [97] pre-induced cross-twinning lamellas on AZ31 magnesium alloys and sequent annealing was conducted at 450°C. The nucleation of new recrystallized grains was promoted by twin-twin intersections. Some of the new grains inherited the orientation of twins. Thus, the position where the internal stress fit the critical energy of DRX can promote the DRX behavior of Mg alloys during deformation. The twin-twin intersection can not only rotate the grains away from basal pole, but also reserve enough energy which can be set as the DRX nucleation sites. The DRXed grains follow the twinning orientation which weakens the basal texture greatly. However, the amount and the position of the twin-twin intersections are difficult to be controlled which need more studies deeply. Besides, compressive or double twins contain more store energy which can set as the DRX nucleation sites independently. However, how the twinning orientation affects the new DRXed grains are not clear which can be investigated thoroughly for texture control.

Above all, pre-twins promote the rotation of Mg alloy grains approximately 86.3° away from the basal plane, and the twinning texture components will be obtained. The grains are divided by the induced twinning lamellas, which also have the function of grain refinement. The twinning rotated orientation and grain refitment favor the activity of basal $\langle a \rangle$ slip, which is beneficial for enhancing the plasticity and strength of Mg alloys. However, most of the pre-twinning processes are conducted on the Mg plate or block with a larger thickness. A new pre-twinning technology is urgently needed for the use of this theory on Mg alloy thin sheets of large size. Detwinning also plays an important role in the texture evolution, which can improve the plasticity of Mg alloys. Detwinning behavior occurs when an inverse tension load is applied to the twined alloys [98,99]. During this process, the orientation of the twinning grains will rotate again to the basal pole. This occurs regardless of the tension or compression deformation of twined Mg alloys [100,101]. However, how to control the texture by detwinning has not been reported, and the mechanism is still unclear. On the other hand, pre-twins can promote the recrystallization of Mg alloys. Both nucleation and grain growth during recrystallization can result in texture recombination and weakening, especially at twinning intersections. However, the amount and the position of the twin-twin intersections are difficult to be controlled which need more studies deeply. The new recrystallized grains will keep the rotated twinning orientations, and a texture-weakened Mg alloy will be obtained. However, the texture modification by grain growth, especially abnormal growth with a critical store energy, needs to be investigated further.

3. Effect of texture control on the plasticity of magnesium alloys

As well known, the slip and twinning are very important during deformation for magnesium alloys. Twinning is a

polar deformation mechanism that can start only in a special loading direction. Similar to (10-12) tensile twinning with a smaller CRSS, the compression/tension loading should be perpendicular to the c-axis of the grains. Otherwise, (10-11) compressive twinning starts. For compressive twinning, the CRSS is relatively higher and difficult to perform. Under this condition, the basal slip is much more important for deformation accommodation at low temperatures. While the basal plane provides only two independent slips, non-basal slip such as prismatic $\langle a \rangle$ and pyramid $\langle a + c \rangle$ slip cannot be activated at room temperature [26,102,103]. The basal plane cannot fit the von Mises stress criterion that requires five independent slips. It also expresses a poor plasticity at lower temperatures, especially lower than the recrystallization temperature (below 150°C in this study). Most of the formations on Mg alloys are conducted at higher temperatures to activate non-basal slips owing to thermal activation. However, the grains grow and the surface quality is quite low. For devices with a special requirement on properties, for example, corrosion or strength, forming at lower temperatures is necessary under this condition. Texture weakening promotes the activity of basal $\langle a \rangle$ slip systems, which can enhance the plasticity significantly; hence, the ductility, stretch formability, workability and so on.

3.1. Ductility

Zhang et al. [57] reported that a preferred orientation consisting of (0001) basal planes aligned with the extrusion axis was obtained in Mg-1.0Zn Mg alloy extrusion billets. However, the double peak (0002) RE-texture was formed in Mg-1.0Zn-xCa alloys. At a higher alloying level of 0.5% Ca, a second texture peak at approximately (11-20) parallel to the extrusion direction was generated due to the activity of non-basal $\langle a + c \rangle$ slip and dynamic recrystallization, so that the basal texture was weakened greatly. This is discussed in the previous section. The basal texture was harmful to ductility, but beneficial to the tensile strength of the alloys, while the non-basal texture was beneficial to the activation of the non-basal slip. Owing to the weakening of basal texture and generation of non-basal texture after the addition of Ca elements, the Schmidt factor of the basal slip increased remarkably. The deformation is usually dominated by basal slip at room temperature. Additionally, the CRSS of non-basal slip may also drop with a tilted basal RE-texture, which also benefits the enhancement of ductility. Therefore, the tensile fracture elongation increased by more than 40% compared to that of Mg-1.0Zn, as shown in Fig. 12. The improvement of ductility through texture weakening induced by Ce element alloying has also been reported, and the fracture elongation can reach more than 30% in Mg-0.2% Ce alloys, for a similar reason [104]. Texture weakening has an important effect on the ductility of the magnesium alloy not only at room temperature but also at warm conditions lower than the recrystallization temperature. Wang et al. [105] conducted an ECAP process at an angle of 110° on AZ80 magnesium alloys at 250°C for various passes. Tension tests were carried out at room temperature, 100°C, and 150°C. The extruded (0002) fiber texture tended to be dominated by 45° rotated texture components, and the intensity decreased as ECAP increased. Owing to texture weakening,

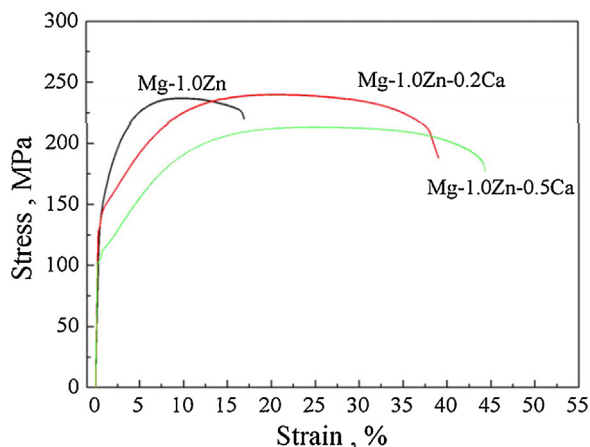


Fig. 13 – Tensile data for extruded Mg and Mg-Zn-xCa alloys [57].

the ductility was improved, especially at 100 °C and 150 °C. The rotated texture favored the activation of basal $\langle a \rangle$ slips so that the fracture elongation improved as ECAP increased. Furthermore, no strain hardening behaviors were exhibited at 150 °C, as shown in Fig. 13. Mg alloys with good plasticity benefit subsequent deformation. The thin-wall microtube of Mg alloys is always processed as a biodegradable intravascular stent. However, this is difficult to perform at room temperature owing to its poor ductility. The grains tend to grow as the

deformation temperature increases, which is harmful for the properties of the generated product, especially for strength and corrosion properties in biodegradable devices [106–108]. Thus, texture-weakened magnesium can be used to produce the thin-wall tube successfully at low temperatures without grain growth. This provides an effective approach to equip magnesium alloys with high plasticity and strength, which can be used to fabricate high-performance Mg products.

3.2. Stretch formability

Texture weakening has a significant effect on the enhancement of stretch formability of Mg alloy sheets. It is well known that width strain can be accommodated by prismatic $\langle a \rangle$ slip, while the strain along the thickness direction can only be coordinated by the pyramidal $\langle a + c \rangle$ slip and twinning in plane deformation on Mg alloy sheets. At room temperature, the pyramidal $\langle a + c \rangle$ slip cannot start. Twinning is a polar mechanism, and the $\{10\text{-}12\}$ tensile twins can only be generated in a specific direction. Thus, there are no slips to coordinate thickness strain in plane deformation, and poor stretch formability is achieved. However, the basal $\langle a \rangle$ slip is enhanced when the basal texture is weakened. The orientation of the grain tilts from ND to ED/RD, favoring the activation of basal slip. The strain along the thickness direction is generated by the basal slips. This is beneficial for improving the stretch formability of Mg alloy sheets. Cai et al. [109] added 0.2 wt.% Y, Ce, Gd elements into Mg-1.5Zn alloys, then hot rolling was carried

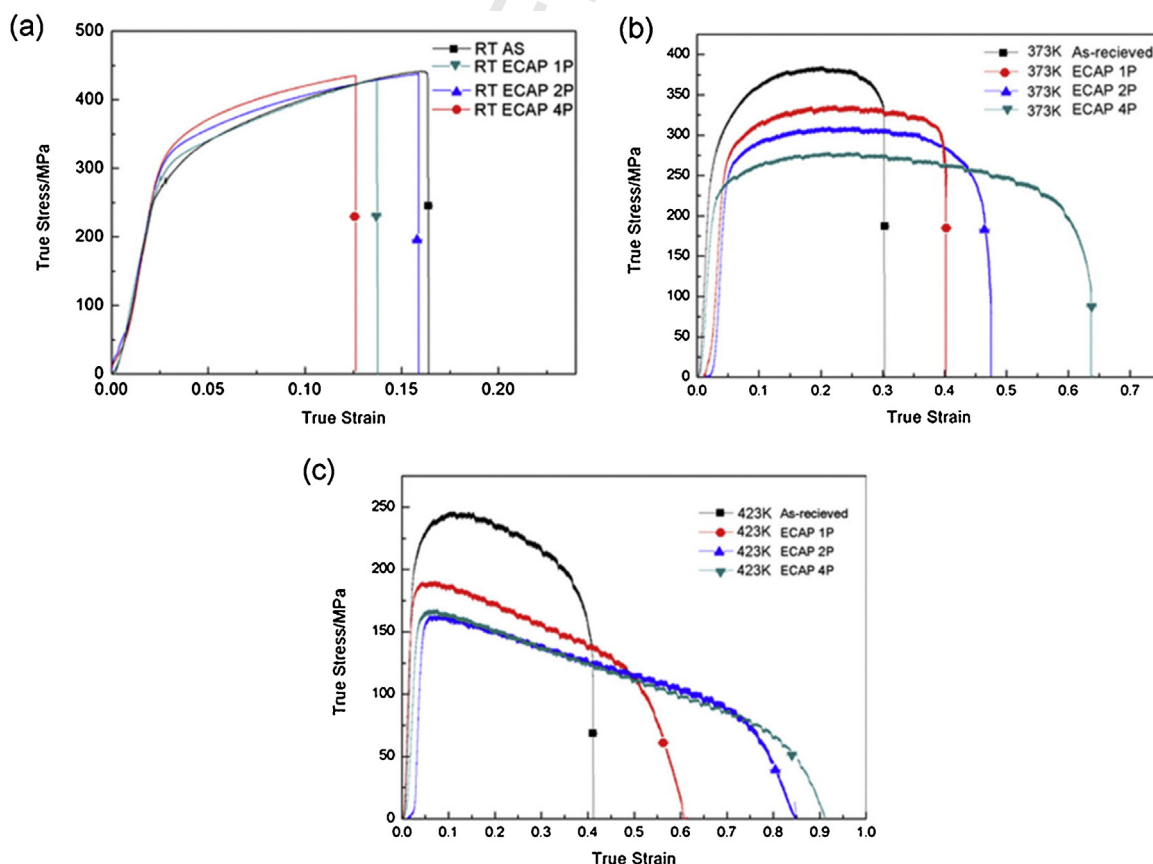


Fig. 14 – The tensile true stress vs. true strain curves of AZ80 alloy processed by ECAP after different passes and tested at different temperatures: (a) room temperature, (b) 100 °C, (c) 150 °C [105].

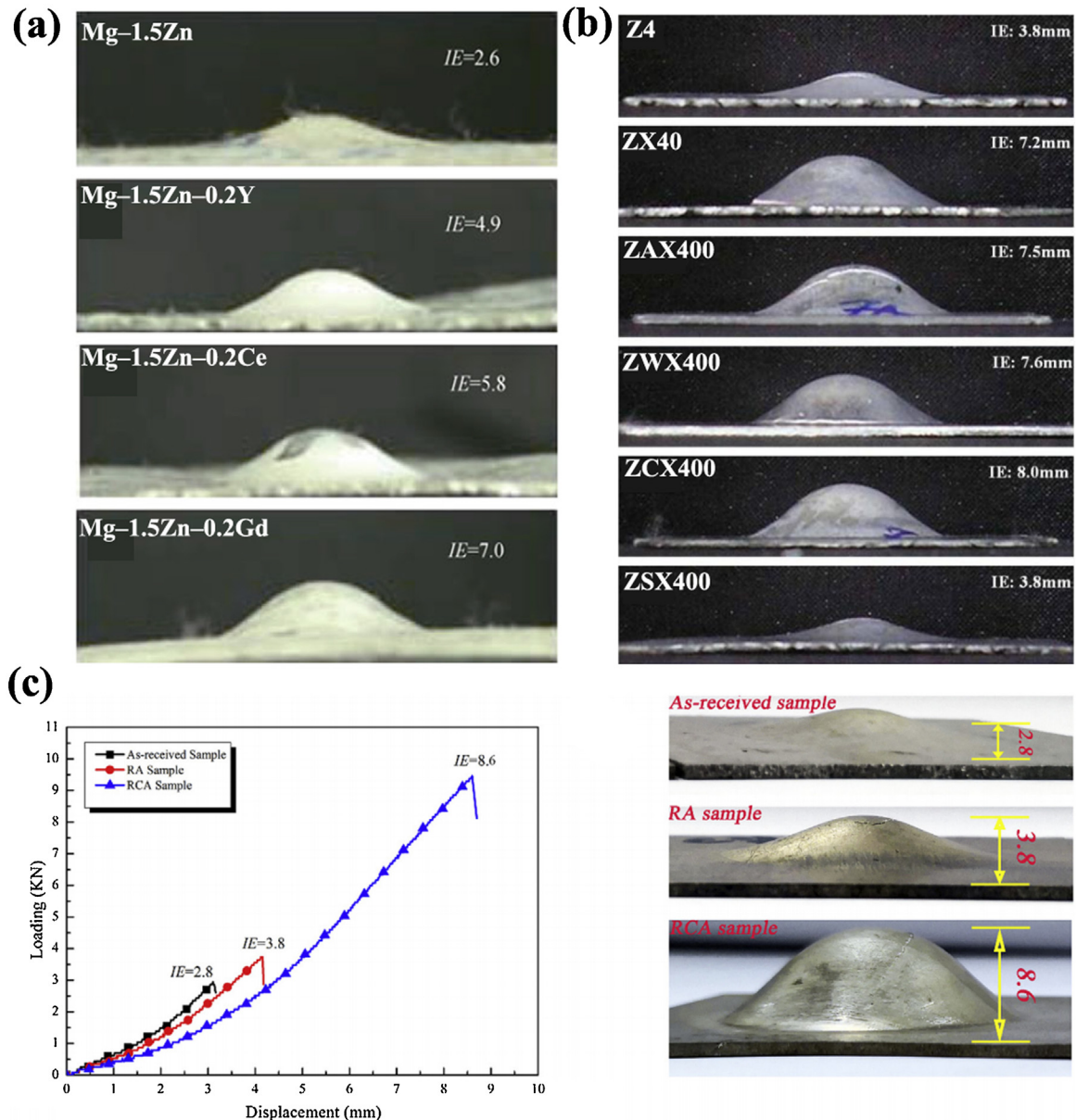


Fig. 15 – The Erichen test samples of various texture weakened Mg alloys at room temperature: (a) Mg-Zn-RE alloys, i Mg-1.5Zn, ii Mg-1.5Zn-0.2Y, iii Mg-1.5Zn-0.2Ce, and iv Mg-1.5Zn-0.2Gd [109]; (b) Mg-4Zn-X-Ca alloys, (i) Z4, (ii) ZX40, (iii) ZAX400, (iv) ZWX400, (v) ZCX400 and (vi) ZSX400 [110]. (c) The room-temperature stretch formability of as-received, RA and RCA samples [111].

976 out at 450 °C and the Mg alloy thin sheet with a thickness of
 977 1 mm was obtained. The RE texture was generated and the
 978 intensity of (0002) basal texture decreased from 13.0 on Mg-
 979 1.5Zn to 2.7, 2.2, and 2.3 on Mg-1.5Zn-0.2Y, Mg-1.5Zn-0.2Ce,
 980 and Mg-1.5Zn-0.2Gd alloys, respectively. Owing to the weak-
 981 ening of the basal texture, the Erichen (IE) values were greatly
 982 enhanced from 2.6 mm to 4.9 mm, 5.8 mm, and 7.0 mm. Simi-
 983 larly, Park et al. [110] reported that the IE values improved
 984 greatly after adding Ca to weaken the basal texture, which
 985 activated the basal < a > slip, as shown in Fig. 14(b). While, the
 986 IE value can be improved by 2.1 times compared with the
 987 as-received samples after pre-twinning on AZ31 Mg alloys
 988 sheet due to an 86.3° rotation of grains [111], as shown in

989 Fig. 14(c). Above all, it is proven that basal texture weaken-
 990 ing is an effective way to enhance the formability of Mg alloy
 991 sheets. However, owing to the double-peak RE texture, the
 992 basal slip can be activated much more easily, which simulta-
 993 neously resulted in a decrease in strength. Usually, the yield
 994 strength can be reduced to even lower than 100 MPa when the
 995 RE texture is dramatically generated [112], as shown in Fig. 15.
 996 This is pernicious and limits the application of Mg sheets on
 997 the other side. Therefore, the balance between formability and
 998 strength should be considered during texture modification.
 999 Bian et al. [113] indicated that there could be a significant
 1000 increase in the flow stress after rapid bake age-hardening on
 1001 texture weakened Mg-1.3Al-0.8Zn-0.7Mn-0.5Ca prior to T4

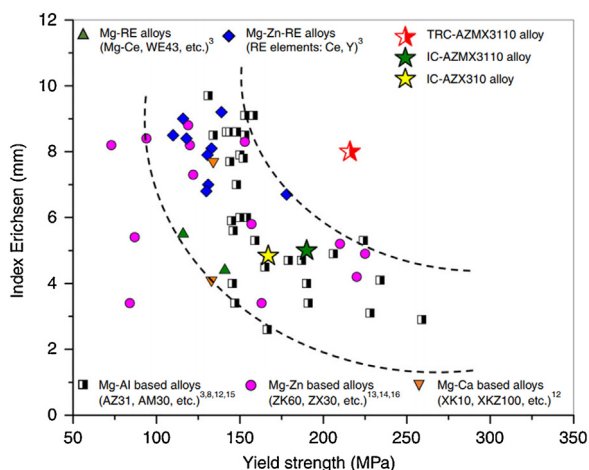


Fig. 16 – Yield strength and stretch formability represented by the index Erichsen (IE) value at room temperature of various Mg alloys sheets [112].

treatment. This enabled the alloy to successfully overcome the strength–formability trade-off dilemma of Mg sheet alloys in the first report. This research direction may be a potential way to consider both properties of heat-treated Mg alloys and can be used for industry applications.

3.3. Processability

The texture not only has significant effects on the ductility and formability, but also plays an important role on the processability of Mg alloys. In general, Mg alloys are used in automobile, 3C shell or degradable devices owing to its special properties. However, the processability is poor because of the crystal structure at lower temperatures. In order to process successfully, the hot forming is conducted at high temper-

atures [114–116]. The grains grow up, which results in poor properties after hot forming according to Hall-petch relationship. Forming at low temperature is necessary for Mg alloys and the texture modifying is a potential way to achieve this goal. Zhang et al. [117,118] conducted repeated unidirectional bending on AZ31 Mg alloy sheet to promote the grain orientation rotation. After annealing, the basal texture was weakened obviously. The results shown that the cellphone shell with good quality was obtained at room temperature while it fractured on as-received AZ31 Mg alloy, as shown in Fig. 16(a). Ge et al. [119,120] indicated that the micro-tube with outer diameter of 4 mm and inner diameter of 3 mm could be formed at 410 °C on AZ31 and ZM21 alloys, and the grains grew up. After ECAP process, it could be done at 150 °C owing to the texture weakening and grain boundary sliding. During which, the grains did not grow up. Thus, the texture control could enhance the processability of Mg alloys. Especially at lower temperature, the softening effect of texture weakening was much more obviously, as shown in Fig. 13, the fracture elongation of 4 passes ECAPed AZ80 Mg alloys was almost 100 % at 150 °C. However, this effect would be reduced when temperature increased, especially above 200 °C, where the non-basal slip might be activated (Fig. 17).

4. Summary and further research directions

Texture control can be considered as a potential way to improve the plasticity of Mg alloys at lower temperatures, especially at low recrystallization temperatures. Many methods have been developed to realize this goal; however, much more work is still needed to further understand the mechanisms or develop new technologies. Current concepts and problems related to texture control can be summarized as follows:

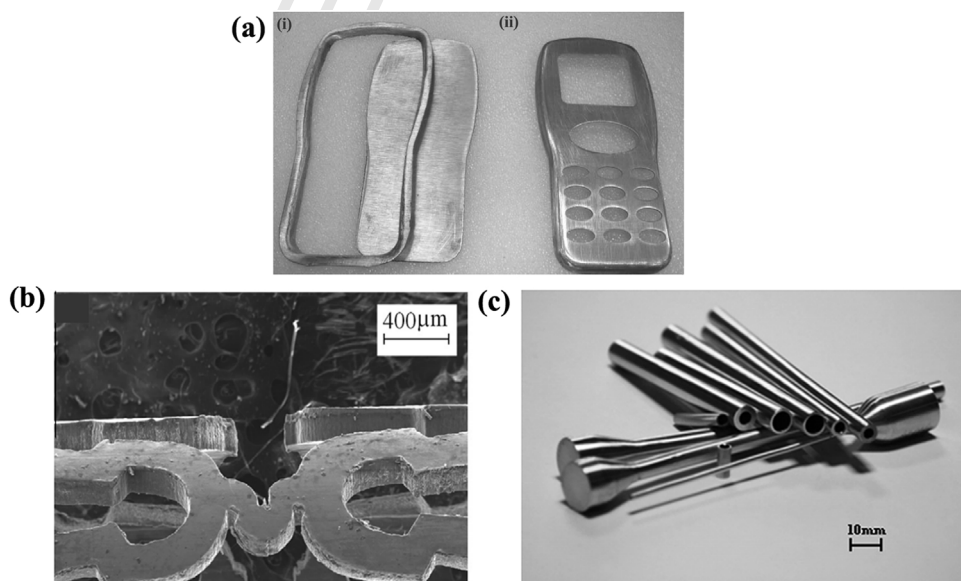


Fig. 17 – The samples of various texture weakened Mg alloys: (a) cold stamping of cell phone housings [117]: (i) as-received sample; (ii) RUB processed specimen; (b) view of the extruded tubes underwent interrupted extrusion at lower temperature [119,120].

- 1046 (1) The split RE-texture can be obtained by alloying both
1047 RE elements and non-RE elements. This is due to the
1048 enhancement of non-basal slip or the effects on the mech-
1049 anisms of DRX, etc. (shear band, twins, particle-stimulated
1050 nucleation, or solar-driven effects). The addition of differ-
1051 ent elements plays different functions, such as decreasing
1052 the stack fault energy or attaining segregation at the grain
1053 boundary. However, general formula generalizations in
1054 texture weakened alloy design are still unclear, especially
1055 for non-RE elements. The effect of added elements on the
1056 stack fault needs more investigations also. In the twinned
1057 Mg alloys, the interactions between the added elements
1058 and the twinning lamellas may play a much more impor-
1059 tant role in texture control, which needs to be investigated
1060 further.
- 1061 (2) The basal pole will be inclined to the shear plane after
1062 introducing shear deformation on Mg alloys. This process
1063 not only refines the grains but also modifies the texture
1064 components. Continuous production of the materials is
1065 a problem. The combination process can be a potential
1066 way for obtaining this target, not only by changing channel
1067 parameters, but also by other factors. Like ASE, this gives
1068 another perspective, which is that the shear deformation
1069 can be introduced by materials flow control, not only by
1070 the different speed metal flow processes, but also by gradi-
1071 ent deformation temperature or friction factors. It is more
1072 effective and convenient to obtain the texture weakened
1073 Mg alloy sheet. However, the gradient microstructure is
1074 also one problem which should be considered to reduce
1075 during fabrication.
- 1076 (3) The orientation of grains can be tilted away from ND by
1077 approximately 86.3° by induced tensile twins, which have
1078 a great potential to weaken the basal texture. Owing to the
1079 polarity of twins, twinning can only be activated along a
1080 special loading direction. Thus, the pre-twinning process
1081 is difficult to conduct on thin Mg sheets. Current technolo-
1082 gies can conduct pre-twinning only to a small extent, and
1083 the deformation may not be uniform. The new continuous
1084 and simple pre-twinning devices on Mg alloy thin sheets
1085 with larger scale should be developed in the future. The
1086 twin-twin intersection can not only rotate the grains, but
1087 also reserve enough energy to be set as the DRX nucle-
1088 ation sites. However, the amount and the position of the
1089 twin-twin intersections are difficult to be controlled which
1090 needs more studies deeply. Besides, compressive or double
1091 twins which can set as the DRX nucleation sites inde-
1092 pendently. How the twinning orientation affects the new
1093 DRXed grains are not clear which can be investigated thor-
1094 oughly for texture control.
- 1095 (4) Detwinning behavior is beneficial for improving the plas-
1096 ticity of Mg alloys under inverse tension loading and will
1097 occur when the inverse load is carried out on the twinned
1098 Mg alloys. Then, the orientation of the grains will rotate
1099 back to the basal pole. However, control of the texture
1100 by detwinning is still unclear. Thus, further research can
1101 focus on developing a new method to pre-twin on a large
1102 scale on thin Mg alloy sheets. Various types of twins, such
1103 as compressive, double twins, and detwinning behavior,
1104 can also be used to weaken the basal texture.
- 1105 (5) Research reveals that the bigger the grains, the more ran-
1106 dom the basal poles will be on the Mg alloy sheet during
1107 the grain growth stage. There is critical store energy to
1108 achieve the largest grain growth rate during DRX. When
1109 the value is exceeded, the grain size decreases, for exam-
1110 ple, a 5% decrease is induced by pre-stretch deformation.
1111 To broaden this application, the critical strain induced by
1112 various processing methods should be clear. The related
1113 grain-growth mechanisms should be investigated thor-
1114 oughly.
- 1115 (6) Owing to the enhanced activity of basal < a > slips by basal
1116 texture weakening, the plasticity, ductility, and the stretch
1117 formability of Mg alloys, can be improved. However, the
1118 strength will be decreased greatly at the same time, espe-
1119 cially in Mg alloys with a split RE texture. Therefore, the
1120 balance between strength and plasticity should be con-
1121 sidered.

Declaration of Interest Statement

- 1 The authors declare that they have no known competing
1122 financial interests or personal relationships that could have
1123 appeared to influence the work reported in this paper.
1124
- 2 The authors declare the following financial inter-
1125 ests/personal relationships which may be considered
1126 as potential competing interests:
1127

Competing financial interests

The authors declare that they have no known competing
1128 financial interests or personal relationships that could have
1129 appeared to influence the work reported in this paper.
1130

Acknowledgements

The authors thank the National Natural Science Founda-
1131 tion of China (51704209, U1810208, U1810122), The Projects of
1132 International Cooperation in Shanxi (201803D421086), Shanxi
1133 Province patent promotion implementation fund (20200718),
1134 the Outstanding Innovative Teams of Higher Learning Institu-
1135 tions of Shanxi (2018), and Technological Innovation Programs
1136 of Higher Education Institutions in Shanxi (201802034), Shanxi
1137 province scientific facilities and instruments shared ser-
1138 vice platform of magnesium-based materials electric impulse
1139 aided forming (201805D141005), Science and Technology
1140 Major Project of Shanxi province (20191102008, 20191102007,
1141 20181101008).
1142

REFERENCES

- [1] Ramalingam VV, Ramasamy P, Kovukkal MD, Myilsamy G.
1145 Research and development in magnesium alloys for
1146 industrial and biomedical applications: a review. *Met Mater*
1147 *Inter* 2019;1-22.
1148
- [2] Zeng Z, Stanford N, Davies CHJ, Nie J-F, Birbilis N.
1149 Magnesium extrusion alloys: a review of developments and
1150 prospects. *Inter Mater Rev* 2019;64(1):27-62.

- 1151 [3] Rashad M, Pan F, Lin D, Asif M. High temperature
1152 mechanical behavior of AZ61 magnesium alloy reinforced
1153 with graphene nanoplatelets. *Mater Des* 2016;89:1242–50.
1154 [4] Huang X, Suzuki K, Chino Y, Mabuchi M. Texture and
1155 stretch formability of AZ61 and AM60 magnesium alloy
1156 sheets processed by high-temperature rolling. *J Alloy*
1157 *Compd* 2015;632:94–102.
1158 [5] Jiang M, Xu C, Yan H, Fan G, Nakata T, Lao C, Chen R,
1159 Kamado S, Han E, Lu B. Unveiling the formation of basal
1160 texture variations based on twinning and dynamic
1161 recrystallization in AZ31 magnesium alloy during
1162 extrusion. *Acta Mater* 2018;157:53–71.
1163 [6] Jiang M, Xu C, Nakata T, Yan H, Chen R, Kamado S. Rare
1164 earth texture and improved ductility in a Mg-Zn-Gd alloy
1165 after high-speed extrusion. *Mater Sci Eng A* 2016;667:233–9.
1166 [7] Zeng Z, Zhu Y, Xu S, Bian M, Davies C, Birbilis N, Nie J.
1167 Texture evolution during static recrystallization of
1168 cold-rolled magnesium alloys. *Acta Mater* 2016;105:479–94.
1169 [8] Jiao F-W, Jin L, Dong J, Wang F-H. In situ electron backscatter
1170 diffraction analysis for microstructure evolution and
1171 deformation models of Mg-Ce alloy during uniaxial loading.
1172 *Acta Metall Sinica (English Lett)* 2019;32(2):263–8.
1173 [9] Dou Y, Luo H, Zhang J, Tang X. Generalized Stacking Fault
1174 Energy of {10-11}<11-23> Slip System in Mg-Based Binary
1175 Alloys: A First Principles Study. *Mater* 2019;12(9):1548.
1176 [10] Tan L, Zhang X, Sun Q, Yu J, Huang G, Liu Q. Pyramidal slips
1177 in high cycle fatigue deformation of a rolled Mg-3Al-1Zn
1178 magnesium alloy. *Mater Sci Eng A* 2017;699:247–53.
1179 [11] Ping Y, Lina W, Xiao L, Li M. Orientation factor analysis of
1180 deformation mechanisms under special processing
1181 techniques in AZ31 magnesium alloys. *Acta Metall Sinica*
1182 *(English Lett)* 2010;23(1):63–71.
1183 [12] Chen W, Wang X, Kyalo MN, Wang E, Liu Z. Yield strength
1184 behavior for rolled magnesium alloy sheets with texture
1185 variation. *Mater Sci Eng A* 2013;580:77–82.
1186 [13] Stanford N, Barnett MR. Solute strengthening of prismatic
1187 slip, basal slip and {1012} twinning in Mg and Mg-Zn binary
1188 alloys. *Inter J Plasticity* 2013;47:165–81.
1189 [14] Blake A, Cáceres C. Solid-solution hardening and softening
1190 in Mg-Zn alloys. *Mater Sci Eng A* 2008;483:161–3.
1191 [15] Koike J. Enhanced deformation mechanisms by anisotropic
1192 plasticity in polycrystalline Mg alloys at room temperature.
1193 *Metall Mater Trans A* 2005;36:1689–96.
1194 [16] Chino Y, Kimura K, Hakamada M, Mabuchi M. Mechanical
1195 anisotropy due to twinning in an extruded AZ31 Mg alloy.
1196 *Mater Sci Eng A* 2008;485:311–7.
1197 [17] Nan X-L, Wang H-Y, Zhang L, Li J-B, Jiang Q-C. Calculation of
1198 Schmid factors in magnesium: Analysis of deformation
1199 behaviors. *Scripta Mater* 2012;67(5):443–6.
1200 [18] Huang X, Suzuki K, Watazu A, Shigematsu I, Saito N.
1201 Mechanical properties of Mg-Al-Zn alloy with a tilted basal
1202 texture obtained by differential speed rolling. *Mater Sci Eng*
1203 *A* 2008;488(1–2):214–20.
1204 [19] Wang R, Eliezer A, Gutman E. An investigation on the
1205 microstructure of an AM50 magnesium alloy. *Mater Sci Eng*
1206 *A* 2003;355(1–2):201–7.
1207 [20] Wang R, Eliezer A, Gutman E. Microstructures and
1208 dislocations in the stressed AZ91D magnesium alloys.
1209 *Mater Sci Eng A* 2003;344(1–2):279–87.
1210 [21] Dong J, Zhang D, Dong Y, Chai S, Pan F. Microstructure
1211 evolution and mechanical response of extruded AZ31B
1212 magnesium alloy sheet at large strains followed by
1213 annealing treatment. *Mater Sci Eng A* 2014;618:262–70.
1214 [22] Xu J, Song J, Jiang B, He J, Wang Q, Liu B, Huang G, Pan F.
1215 Effect of effective strain gradient on texture and mechanical
1216 properties of Mg-3Al-1Zn alloy sheets produced by
1217 asymmetric extrusion. *Mater Sci Eng A* 2017;706:172–80.
1218 [23] Wang L, Zhang Z, Cao M, Zhang H, Han T, Wang H,
1219 Arthanari S, Cheng W, Jinlong L. Enhanced Stretch
1220 Formability of Magnesium Alloy Sheet by Prestretching at
1221 Various Speeds at Higher Temperature. *JOM*
1222 2019;71(5):1705–13.
1223 [24] Guo F, Zhang D, Yang X, Jiang L, Chai S, Pan F. Effect of
1224 rolling speed on microstructure and mechanical properties
1225 of AZ31 Mg alloys rolled with a wide thickness reduction
1226 range. *Mater Sci Eng A* 2014;619:66–72.
1227 [25] Guan D, Wynne B, Gao J, Huang Y, Rainforth WM. Basal slip
1228 mediated tension twin variant selection in magnesium
1229 WE43 alloy. *Acta Mater* 2019;170:1–14.
1230 [26] Kim S-J, Lee C, Koo J, Lee J, Lee Y-S, Kim D. Improving the
1231 room-temperature formability of a magnesium alloy sheet
1232 by texture control. *Mater Sci Eng A* 2018;724:156–63.
1233 [27] Yang P, Yu Y, Chen L, Mao W. Experimental determination
1234 and theoretical prediction of twin orientations in
1235 magnesium alloy AZ31. *Scripta Mater* 2004;50(8):1163–8.
1236 [28] Qian X, Zeng Y, Jiang B, Dou Y, Shi O, Quan G, Li B, Pan F.
1237 Study on mechanical behaviors and theoretical critical
1238 shear strength of cold-rolled AZ31 alloy with different Li
1239 additions. *Mater Sci Eng A* 2019;742:241–54.
1240 [29] Li C-j, H-f Sun, Li X-w, J-l Zhang, W-b Fang, Z-y Tan.
1241 Microstructure, texture and mechanical properties of
1242 Mg-3.0 Zn-0.2 Ca alloys fabricated by extrusion at various
1243 temperatures. *J Alloys Compd* 2015;652:122–31.
1244 [30] Sanjari M, Kabir ASH, Farzadfar A, Utsunomiya H, Petrov R,
1245 Kestens L, Yue S. Promotion of texture weakening in
1246 magnesium by alloying and thermomechanical processing.
1247 II: rolling speed. *J Mater Sci* 2014;49:1426–36.
1248 [31] Wu J, Jin L, Dong J, Wang F, Dong S. The texture and its
1249 optimization in magnesium alloy. *J Mater Sci Technol*
1250 2020;42:175–89.
1251 [32] Chen Y, Jin L, Dong J, Zhang Z, Wang F. Twinning effects on
1252 the hot deformation behavior of AZ31 Mg alloy. *Mater*
1253 *Charact* 2016;118:363–9.
1254 [33] Xin Y, Wang M, Zeng Z, Huang G, Liu Q. Tailoring the texture
1255 of magnesium alloy by twinning deformation to improve
1256 the rolling capability. *Scripta Mater* 2011;64(10):986–9.
1257 [34] Liu P, Jiang H, Cai Z, Kang Q, Zhang Y. The effect of Y, Ce and
1258 Gd on texture, recrystallization and mechanical property of
1259 Mg-Zn alloys. *J Magnes Alloys* 2016;4(3):188–96.
1260 [35] Stanford N. Micro-alloying Mg with Y, Ce, Gd and La for
1261 texture modification—A comparative study. *Mater Sci Eng A*
1262 2010;527(10–11):2669–77.
1263 [36] Kula A, Jia X, Mishra R, Niewczas M. Flow stress and work
1264 hardening of Mg-Y alloys. *Inter J Plasti* 2017;92:96–121.
1265 [37] Shi B, Chen R, Ke W. Effects of yttrium and zinc on the
1266 texture, microstructure and tensile properties of hot-rolled
1267 magnesium plates. *Mater Sci Eng A* 2013;560:62–70.
1268 [38] Wu B, Zhao Y, Du X, Zhang Y, Wagner F, Esling C. Ductility
1269 enhancement of extruded magnesium via yttrium addition.
1270 *Mater Sci Eng A* 2010;527(16–17):4334–40.
1271 [39] Agnew S, Yoo M, Tome C. Application of texture simulation
1272 to understanding mechanical behavior of Mg and solid
1273 solution alloys containing Li or Y. *Acta Mater*
1274 2001;49(20):4277–89.
1275 [40] Sandlöbes S, Zaefferer S, Schestakow I, Yi S,
1276 Gonzalez-Martinez R. On the role of non-basal deformation
1277 mechanisms for the ductility of Mg and Mg-Y alloys. *Acta*
1278 *Mater* 2011;59(2):429–39.
1279 [41] Griffiths D. Explaining texture weakening and improved
1280 formability in magnesium rare earth alloys. *Mater Sci*
1281 *Technol* 2015;31(1):10–24.
1282 [42] Mishra RK, Brahme A, Sabat RK, Jin L, Inal K. Twinning and
1283 texture randomization in Mg and Mg-Ce alloys. *Inter Jo*
1284 *Plastic* 2019;117:157–72.

- 1285 [43] Masoumi M, Hoseini M, Pekguleryuz M. The influence of Ce
1286 on the microstructure and rolling texture of Mg–1% Mn
1287 alloy. *Mater Sci Eng A* 2011;528(7-8):3122–9. 1355
- 1288 [44] Chino Y, Kado M, Mabuchi M. Enhancement of tensile
1289 ductility and stretch formability of magnesium by addition
1290 of 0.2 wt%(0.035 at%) Ce. *Mater Sci Eng A*
1291 2008;494(1–2):343–9. 1356
- 1292 [45] Wang Q, Du W, Liu K, Wang Z, Li S, Wen K. Microstructure,
1293 texture and mechanical properties of as-extruded
1294 Mg–Zn–Er alloys. *Mater Sci Eng A* 2013;581:31–8. 1357
- 1295 [46] Yu H, Park SH, You BS, Kim YM, Yu H, Park SH. Effects of
1296 extrusion speed on the microstructure and mechanical
1297 properties of ZK60 alloys with and without 1 wt% cerium
1298 addition. *Mater Sci Eng A* 2013;583:25–35. 1358
- 1299 [47] Wu D, Chen R, Han E. Excellent room-temperature ductility
1300 and formability of rolled Mg–Gd–Zn alloy sheets. *J Alloys*
1301 *Compd* 2011;509(6):2856–63. 1359
- 1302 [48] Yan H, Xu S, Chen R, Kamado S, Honma T, Han E. Twins,
1303 shear bands and recrystallization of a Mg–2.0% Zn–0.8% Gd
1304 alloy during rolling. *Scripta Mater* 2011;64(2):141–4. 1360
- 1305 [49] Stanford N, Atwell D, Barnett MR. The effect of Gd on the
1306 recrystallisation, texture and deformation behaviour of
1307 magnesium-based alloys. *Acta Mater* 2010;58(20):6773–83. 1361
- 1308 [50] Wu W, Jin L, Wang F, Sun J, Zhang Z, Ding W, Dong J.
1309 Microstructure and texture evolution during hot rolling and
1310 subsequent annealing of Mg–1Gd alloy. *Mater Sci Eng A*
1311 2013;582:194–202. 1362
- 1312 [51] Xu X, Chen X, Du W, Geng Y, Pan F. Effect of Nd on
1313 microstructure and mechanical properties of as-extruded
1314 Mg–Y–Zr–Nd alloy. *J Mater Sci Technol* 2017;33(9):926–34. 1363
- 1315 [52] Hantzsche K, Bohlen J, Wendt J, Kainer K, Yi S, Letzig D.
1316 Effect of rare earth additions on microstructure and texture
1317 development of magnesium alloy sheets. *Scripta Mater*
1318 2010;63(7):725–30. 1364
- 1319 [53] Hadorn JP, Hantzsche K, Yi S, Bohlen J, Letzig D,
1320 Wollmershauser JA, Agnew SR. Role of solute in the texture
1321 modification during hot deformation of Mg–rare earth
1322 alloys. *Metall Mater Trans A* 2012;43(4):1347–62. 1365
- 1323 [54] Zengin H, Turen Y. Effect of La content and extrusion
1324 temperature on microstructure, texture and mechanical
1325 properties of Mg–Zn–Zr magnesium alloy. *Mater Chem Phys*
1326 2018;214:421–30. 1366
- 1327 [55] Sadeghi A, Pekguleryuz M. Microstructure, mechanical
1328 properties and texture evolution of AZ31 alloy containing
1329 trace levels of strontium. *Mater Charact* 2011;62(8):742–50. 1367
- 1330 [56] Wang G, Huang G, Chen X, Deng Q, Tang A, Jiang B, Pan F.
1331 Effects of Zn addition on the mechanical properties and
1332 texture of extruded Mg–Zn–Ca–Ce magnesium alloy sheets.
1333 *Mater Sci Eng A* 2017;705:46–54. 1368
- 1334 [57] Zhang B, Wang Y, Geng L, Lu C. Effects of calcium on texture
1335 and mechanical properties of hot-extruded Mg–Zn–Ca
1336 alloys. *Mater Sci Eng A* 2012;539:56–60. 1369
- 1337 [58] Li R, Pan F, Jiang B, Dong H, Yang Q. Effect of Li addition on
1338 the mechanical behavior and texture of the as-extruded
1339 AZ31 magnesium alloy. *Mater Sci Eng A* 2013;562:33–8. 1370
- 1340 [59] Yuasa M, Hayashi M, Mabuchi M, Chino Y. Improved plastic
1341 anisotropy of Mg–Zn–Ca alloys exhibiting high-stretch
1342 formability: A first-principles study. *Acta Mater*
1343 2014;65:207–14. 1371
- 1344 [60] Agnew S, Mehrotra P, Lillo T, Stoica G, Liaw P. Texture
1345 evolution of five wrought magnesium alloys during route A
1346 equal channel angular extrusion: Experiments and
1347 simulations. *Acta Mater* 2005;53(11):3135–46. 1372
- 1348 [61] Naik GM, Sannayellappa N, Kumar SSS. Corrosion of
1349 ECAPed Magnesium alloys and its background: A review.
1350 *JOM* 2019;29(2). 1373
- 1351 [62] Varadala AB, Gurugubelli SN, Bandaru S. Enhancement of
1352 structural and mechanical behavior of Al–Mg alloy
1353 processed by ECAE. *Mater Today Proceedings*
1354 2019;18:2147–51. 1374
- [63] Wang X-S, Jin L, Li Y, Guo X-W. Effect of equal channel
angular extrusion process on deformation behaviors of
Mg–3Al–Zn alloy. *Mater Lett* 2008;62(12–13):1856–8. 1375
- [64] Li XB, Li F, Li XB. Effect of different temperatures on
deformation characteristics of AZ31 magnesium alloy by
continuous variable cross-section direct extrusion. *Inter J*
Advanced Manuf Technol 2018;95(9–12):
4623–8. 1376
- [65] Hu H, Wang H, Zhai Z, Li Y, Fan J, Ou Z. Effects of channel
angles on extrusion-shear for AZ31 magnesium alloy:
modeling and experiments. *Inter J Advanced Manuf Technol*
2015;76(9–12):1621–30. 1377
- [66] Liu X-Y, Lu L-W, Sheng K, Zhou T. Microstructure and
Texture Evolution During the Direct Extrusion and
Bending–Shear Deformation of AZ31 Magnesium Alloy.
Acta Metall Sinica (Eng Lett) 2019;32(6):710–8. 1378
- [67] Faraji G, Yavari P, Aghdamifar S, Mashhadi MM. Mechanical
and microstructural properties of ultra-fine grained AZ91
magnesium alloy tubes processed via multi pass Tubular
Channel Angular Pressing (TCAP). *J Mater Sci Technol*
2014;30(2):134–8. 1379
- [68] Hu H, Qin X, Zhang D, Ma X. A novel severe plastic
deformation method for manufacturing AZ31 magnesium
alloy tube. *Inter J Advanced Manuf Technol*
2018;98(1-4):897–903. 1380
- [69] Huang X, Suzuki K, Watazu A, Shigematsu I, Saito N.
Microstructural and textural evolution of AZ31 magnesium
alloy during differential speed rolling. *J Alloys Compd*
2009;479(1-2):726–31. 1381
- [70] Huang X, Suzuki K, Saito N. Textures and stretch formability
of Mg–6Al–1Zn magnesium alloy sheets rolled at high
temperatures up to 793 K. *Scripta Mater* 2009;60(8):651–4. 1382
- [71] Huang X, Suzuki K, Saito N. Microstructure and mechanical
properties of AZ80 magnesium alloy sheet processed by
differential speed rolling. *Mater Sci Eng A*
2009;508(1-2):226–33. 1383
- [72] Del Valle J, Pérez-Prado MT, Ruano OA. Texture evolution
during large-strain hot rolling of the Mg AZ61 alloy. *Mater*
Sci Eng A 2003;355(1-2):68–78. 1384
- [73] Hamad K, Ko YG. A cross-shear deformation for optimizing
the strength and ductility of AZ31 magnesium alloys. *Sci*
Rep 2016;6(1):1–8. 1385
- [74] Song D, Zhou T, Tu J, Shi L, Song B, Hu L, Yang M, Chen Q, Lu
L. Improved stretch formability of AZ31 sheet via texture
control by introducing a continuous bending channel into
equal channel angular rolling. *J Mater Process Technol*
2018;259:380–6. 1386
- [75] Yang Q, Jiang B, Tian Y, Liu W, Pan F. A tilted weak texture
processed by an asymmetric extrusion for magnesium alloy
sheets. *Materials Letters* 2013;100:29–31. 1387
- [76] Yang Q, Jiang B, He J, Song B, Liu W, Dong H, Pan F. Tailoring
texture and refining grain of magnesium alloy by
differential speed extrusion process. *Mater Sci Eng A*
2014;612:187–91. 1388
- [77] Yang Q, Jiang B, Pan H, Song B, Jiang Z, Dai J, Wang L, Pan F.
Influence of different extrusion processes on mechanical
properties of magnesium alloy. *J Magnes Alloys*
2014;2(3):220–4. 1389
- [78] Huo Q, Yang X, Sun H, Li B, Qin J, Wang J, Ma J.
Enhancement of tensile ductility and stretch formability of
AZ31 magnesium alloy sheet processed by cross-wavy
bending. *J Alloys Compd* 2013;581:230–5. 1390
- [79] Zhang H, Huang G, Kong D, Sang G, Song B. Influence of
initial texture on formability of AZ31B magnesium alloy
sheets at different temperatures. *J Mater Process Technol*
2011;211(10):1575–80. 1391

- 1421 [80] Song B, Huang G, Li H, Zhang L, Huang G, Pan F. Texture
1422 evolution and mechanical properties of AZ31B magnesium
1423 alloy sheets processed by repeated unidirectional bending. *J*
1424 *Alloys Compd* 2010;489(2):475–81. 1490
- 1425 [81] Zhang H, Huang G, Fan J, Roven HJ, Xu B, Dong H. Deep
1426 drawability and drawing behaviour of AZ31 alloy sheets
1427 with different initial texture. *J Alloys Compd*
1428 2014;615:302–10. 1491
- 1429 [82] Hou D, Liu T, Luo L, Lu L, Chen H, Shi D. Twinning behaviors
1430 of a rolled AZ31 magnesium alloy under multidirectional
1431 loading. *Mater Charact* 2017;124:122–8. 1492
- 1432 [83] Wang L, Huang G, Quan Q, Bassani P, Mostaed E, Vedani M,
1433 Pan F. The effect of twinning and detwinning on the
1434 mechanical property of AZ31 extruded magnesium alloy
1435 during strain-path changes. *Mater Des* 2014;63:
1436 177–84. 1493
- 1437 [84] Song L, Wu B, Zhang L, Du X, Wang Y, Esling C. Twinning
1438 characterization of fiber-textured AZ31B magnesium alloy
1439 during tensile deformation. *Mater Sci Eng A* 2018;710:57–65. 1494
- 1440 [85] Hou D, Liu T, Shi M, Wen H, Zhao H. Deformation
1441 Mechanisms in a Rolled Magnesium Alloy Under Tension
1442 Along the Rolling Direction. *Microsc Microanal*
1443 2018;24(3):207–13. 1495
- 1444 [86] Song B, Xin R, Chen G, Zhang X, Liu Q. Improving tensile
1445 and compressive properties of magnesium alloy plates by
1446 pre-cold rolling. *Scripta Mater* 2012;66(12):1061–4. 1496
- 1447 [87] Xin Y, Wang M, Zeng Z, Nie M, Liu Q. Strengthening and
1448 toughening of magnesium alloy by {1 0–1 2} extension
1449 twins. *Scripta Mater* 2012;66(1):25–8. 1497
- 1450 [88] Park SH, Hong S-G, Lee CS. Enhanced stretch formability of
1451 rolled Mg–3Al–1Zn alloy at room temperature by initial
1452 {10–12} twins. *Mater Sci Eng A* 2013;578:271–6. 1498
- 1453 [89] Wang L, Song B, Zhang Z, Zhang H, Han T, Cao X, Wang H,
1454 Cheng W. Enhanced Stretch Formability of AZ31
1455 Magnesium Alloy Thin Sheet by Induced Precompression
1456 and Sequent Annealing. *Mater* 2018;11(8):
1457 1401. 1499
- 1458 [90] Kim S-J, Kim S-J, Lee K, Cho H-H, Han HN.
1459 Residual-stress-induced grain growth of twinned grains
1460 and its effect on formability of magnesium alloy sheet at
1461 room temperature. *Mater Charact* 2015;109:88–94. 1500
- 1462 [91] Basu I, Al-Samman T. Triggering rare earth texture
1463 modification in magnesium alloys by addition of zinc and
1464 zirconium. *Acta Mater* 2014;67:116–33. 1501
- 1465 [92] Zeng Z, Bian M, Xu S, Davies C, Birbilis N, Nie J. Effects of
1466 dilute additions of Zn and Ca on ductility of magnesium
1467 alloy sheet. *Mater Sci Eng A* 2016;674:459–71. 1502
- 1468 [93] Al-Samman T. Modification of texture and microstructure
1469 of magnesium alloy extrusions by particle-stimulated
1470 recrystallization. *Mater Sci Eng A* 2013;560:
1471 561–6. 1503
- 1472 [94] Zhang H, Huang G, Wang L, Li J. Improved formability of
1473 Mg–3Al–1Zn alloy by pre-stretching and annealing. *Scripta*
1474 *Mater* 2012;67(5):495–8. 1504
- 1475 [95] Xin Y, Zhou H, Yu H, Hong R, Zhang H, Liu Q. Controlling the
1476 recrystallization behavior of a Mg–3Al–1Zn alloy containing
1477 extension twins. *Mater Sci Eng A* 2015;622:178–83. 1505
- 1478 [96] Yu Q, Wang J, Jiang Y, McCabe RJ, Li N, Tomé CN. Twin–twin
1479 interactions in magnesium. *Acta Mater* 2014;77:28–42. 1506
- 1480 [97] Cheng W, Wang L, Zhang H, Cao X. Enhanced stretch
1481 formability of AZ31 magnesium alloy thin sheet by
1482 pre-crossed twinning lamellas induced static
1483 recrystallizations. *J Mater Process Technol* 2018;254:
1484 302–9. 1507
- 1485 [98] Sarker D, Chen D. Dependence of compressive deformation
1486 on pre-strain and loading direction in an extruded
1487 magnesium alloy: Texture, twinning and de-twinning.
1488 *Mater Sci Eng A* 2014;596:134–44. 1508
- [99] Sarker D, Friedman J, Chen D. Influence of pre-strain on
de-twinning activity in an extruded AM30 magnesium
alloy. *Mater Sci Eng A* 2014;605:73–9. 1509
- [100] Zhang H, Jérusalem A, Salvati E, Papadaki C, Fong KS, Song
X, Korsunsky AM. Multi-scale mechanisms of
twinning-detwinning in magnesium alloy AZ31B simulated
by crystal plasticity modeling and validated via in situ
synchrotron XRD and in situ SEM-EBSD. *Inter J Plast*
2019;119:43–56. 1510
- [101] Huang H, Godfrey A, Liu W, Zheng JP. Effect of slip on
detwinning behavior during multi-direction compression of
a wrought magnesium alloy. *Mater Lett* 2016;178:
208–12. 1511
- [102] Li J, Wu D, Chen R, Han E. Anomalous effects of strain rate
on the room-temperature ductility of a cast Mg-Gd-Y-Zr
alloy. *Acta Mater* 2018;159:31–45. 1512
- [103] Ahmad R, Wu Z, Groh S, Curtin W. Pyramidal II to basal
transformation of c+ a edge dislocations in Mg-Y alloys.
Scripta Mater 2018;155:114–8. 1513
- [104] Mishra RK, Gupta AK, Rao PR, Sachdev AK, Kumar AM, Luo
AA. Influence of cerium on the texture and ductility of
magnesium extrusions. *Scripta Mater* 2008;59(5):562–5,
<http://dx.doi.org/10.1016/j.scriptamat.2008.05.019>. 1514
- [105] Wang L, Mostaed E, Cao X, Huang G, Fabrizi A, Bonollo F, Chi
C, Vedani M. Effects of texture and grain size on mechanical
properties of AZ80 magnesium alloys at lower
temperatures. *Mater Des* 2016;89:1–8. 1515
- [106] Mostaed E, Hashempour M, Fabrizi A, Dellasega D, Bestetti
M, Bonollo F, Vedani M. Microstructure, texture evolution,
mechanical properties and corrosion behavior of ECAP
processed ZK60 magnesium alloy for biodegradable
applications. *J Mech Behav Biomed Mater* 2014;37:
307–22. 1516
- [107] Mostaed E, Vedani M, Hashempour M, Bestetti M. Influence
of ECAP process on mechanical and corrosion properties of
pure Mg and ZK60 magnesium alloy for biodegradable stent
applications. *Biomater* 2014;4(1):e28283. 1517
- [108] Mostaed E, Fabrizi A, Dellasega D, Bonollo F, Vedani M. Grain
size and texture dependence on mechanical properties,
asymmetric behavior and low temperature superplasticity
of ZK60 Mg alloy. *Mater Charact* 2015;107:70–8. 1518
- [109] Cai Z-X, Jiang H-T, Tang D, Ma Z, Kang Q. Texture and
stretch formability of rolled Mg–Zn–RE (Y, Ce, and Gd) alloys
at room temperature. *Rare Metal* 2013;32(5):441–7. 1519
- [110] Park SJ, Jung HC, Shin KS. Deformation behaviors of twin roll
cast Mg–Zn–X–Ca alloys for enhanced room-temperature
formability. *Mater Sci Eng A* 2017;679:329–39. 1520
- [111] Yang Q, Jiang B, Wang L, Dai J, Zhang J, Pan F. Enhanced
formability of a magnesium alloy sheet via in-plane
pre-strain paths. *J Alloys Compd* 2020;814:152278. 1521
- [112] Trang T, Zhang J, Kim J, Zargarani A, Hwang J, Suh B-C, Kim
N. Designing a magnesium alloy with high strength and
high formability. *Nat Commun* 2018;9(1):2522. 1522
- [113] Bian M, Sasaki T, Nakata T, Yoshida Y, Kawabe N, Kamado S,
Hono K. Bake-hardenable Mg–Al–Zn–Mn–Ca sheet alloy
processed by twin-roll casting. *Acta Mater* 2018;158:
278–88. 1523
- [114] Cao Z, Wang F, Wan Q, Zhang Z, Jin L, Dong J. Microstructure
and mechanical properties of AZ80 magnesium alloy tube
fabricated by hot flow forming. *Mater Des* 2015;67:
64–71. 1524
- [115] Wang L, Fang G, Qian L, Leeflang S, Duszczynski J, Zhou J.
Forming of magnesium alloy microtubes in the fabrication
of biodegradable stents. *Prog Nat Sci Mater Inter*
2014;24(5):500–6. 1525
- [116] Mei Z, He Y, Jing G, Wang X-x. Review on hot spinning for
difficult-to-deform lightweight metals. *T Nonferr Metal Soc*
2015;25(6):1732–43. 1526

- 1557 [117] Zhang L, Huang G, Zhang H, Song B. Cold stamping 1563
1558 formability of AZ31B magnesium alloy sheet undergoing 1564
1559 repeated unidirectional bending process. *J Mater Process* 1565
1560 *Technol* 2011;211(4):644–9. 1566
1561 [118] Huang G-S, Zhang L, Bo S, Pan F-S. Cold stamping for AZ31B 1567
1562 magnesium alloy sheet of cell phone house. *T Nonferr* 1568
Metal Soc 2010;20:s608–12.
- [119] Ge Q, Dellasega D, Demir AG, Vedani M. The processing of
ultrafine-grained Mg tubes for biodegradable stents. *Acta*
Biomater 2013;9(10):8604–10.
- [120] Ge Q, Vedani M, Vimercati G. Extrusion of magnesium tubes
for biodegradable stent precursors. *Mater Manuf Process*
2012;27(2):140–6.

UNCORRECTED PROOF